$Ti_3C_2T_x$ MXenes-based Electrocatalysts for Enhanced Hydrogen Evolution Reaction (HER)

By

Iqra Mubeen

School of Chemical and Materials Engineering

National University of Sciences and Technology

2023

$Ti_3C_2T_x$ MXenes-based Electrocatalysts for Enhanced Hydrogen Evolution Reaction (HER)

Name: Iqra Mubeen

Reg: 00000361100

This thesis is submitted as a partial fulfillment of the requirements for the degree of

MS in Chemical Engineering

Supervisor Name: Dr. Erum Pervaiz

School of Chemical and Materials Engineering (SCME)
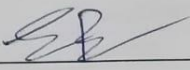
National University of Sciences and Technology (NUST)

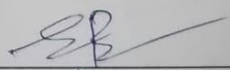**H-12 Islamabad, Pakistan**

July, 2023

THESIS ACCEPTANCE CERTIFICATE

Certified that final copy of MS thesis written by Ms **Iqra Mubeen** (Registration No J0000361100), of School of Chemical & Materials Engineering (SCME) has been vetted by undersigned, found complete in all respects as per NUST Statues/Regulations, is free of plagiarism, errors, and mistakes and is accepted as partial fulfillment for award of MS degree. It is further certified that necessary amendments as pointed out by GEC members of the scholar have also been incorporated in the said thesis.
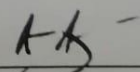
Signature: _____

Name of Supervisor: **Dr Erum Pervaiz**

Date: _____ 22|8|23 _____

Signature (HOD): _____

Date: _____ 22|8|23 _____

Signature (Dean/Principal): _____

Date: _____ 22-8- 2023 _____

National University of Sciences & Technology (NUST)

MASTER'S THESIS WORK

Formulation of Guidance and Examination Committee (GEC)

Name: Iqra Mubeen   NUST Reg No: 00000361100

Department: Department of Chemical Engineering   Specialization: Master of Science in Chemical Engineering

Credit Hour Completed: 24.0   CGPA: 3.69

Course Work Completed

S/No:	Code:	Title:	Core/Elective:	CH:	Grade:
1.	CHE-843	Separation Processes In Che	Compulsory	3.0	A
2.	CHE-847	Chemical Kinetics& Reactor Design	Compulsory	3.0	A
3.	RM-898	Research Methodology	Additional	2.0	Q
4.	CHE-848	Gasification Processes	Elective	3.0	B+
5.	EME-921	Momentum Heat & Mass Transfer In CHE	Compulsory	3.0	B+
6.	CHE-853	Green Process Engineering	Elective	3.0	B+
7.	CHE-823	Advance Analytical Techniques	Elective	3.0	B+
8.	ENE-809	Waste Water Treatment & Design	Elective	3.0	A
9.	ESE-904	Advanced Energy Materials: Synthesis & Characterization	Elective	3.0	B+

Date 03 - Feb - 2023   Student's Signature

Thesis Committee

1. Name: Erum Pervaiz (Supervisor)   Signature
   Department: Department of Chemical Engineering

2. Name: Waheed Miran (Internal)   Signature
   Department: Department of Chemical Engineering

3. Name: Dr.Ameen Shahid (Internal)   Signature
   Department: Department of Chemical Engineering

4. Name: Umair Sikander (Internal)   Signature
   Department: Department of Chemical Engineering

Date: 03 - Feb - 2023   Signature of Head of Department:

APPROVAL

Date: 03 - Feb - 2023   Signature of Dean/Principal:

School of Chemical & Materials Engineering (SCME) (SCME) H-12 Campus,

National University of Sciences &Technology (NUST)

MASTER'S THESIS WORK

We hereby recommend that the dissertation prepared under our supervision by

Regn No & Name: 00000361100 Iqra Mubeen

Title: Ti$_3$C$_2$T$_x$ MXenes-based Electrocatalysts for Enhanced Hydrogen Evolution Reaction (HER).

Presented on: 15 Aug 2023   at: 1400 hrs in SCME Seminar Hall

Be accepted in partial fulfillment of the requirements for the award of Master of Science degree in Chemical Engineering.

Guidance & Examination Committee Members

Name: **Dr Waheed Miran**   Signature: _____

Name: **Dr Ameen Shahid**   Signature: _____

Name: **Dr Umair Sikandar**   Signature: _____

Supervisor's Name: **Dr Erum Pervaiz**   Signature: _____

Dated: 15/8/23

Head of Department
Date 16/8/23

Dean/Principal
Date 18-8-mz3

School of Chemical &Materials Engineering (SCME)

Dedication

Dedicated to my loving parents, respected teachers, to my family and friends.

Acknowledgment

Praise be to Allah the Almighty, the most Gracious and the most Merciful, foremost I must acknowledge my limitless thanks to Allah Almighty, for His help and blessings by giving me the opportunity, courage, and enough energy to carry out and complete the entire thesis work. Then, praises are also addressed to our Prophet Muhammad (PBUH) who has guided us to the better life today. I would like to express my sincere gratitude to my supervisor, Dr. Erum Pervaiz for her invaluable guidance and support throughout my MS program. Her expertise and encouragement helped me to complete this research and write this thesis. I would also like to thank Dr. Waheed Miran, Dr. Ameen Shahid, and Dr. Umair Sikandar for serving on my thesis guidance committee and providing helpful feedback and suggestions. I am grateful to Lt. Col. Saleem Shah (Pak Army) for all the resources and support he provided. This work would not have been possible without his contribution. I would also like to thank my loving parents, and my brothers for their love and support during this process. Without them, this journey would not have been accomplished.

(Iqra Mubeen)

Abstract

Molecular hydrogen (H_2) is the most promising candidate for replacing fossil fuels because of its high energy density and zero carbon emission. Cleaner ways for hydrogen production are highly expected. Electrocatalytic hydrogen evolution reaction (HER) serves for this purpose. Developing highly efficient HER electrocatalysts to minimize the overpotential and facilitate the reaction kinetics is one of the prerequisites to electrocatalytic hydrogen production in large-scale. The research is based on a synthesis of MXenes/MOFs composites for enhanced electrocatalytic HER. $Ti_3C_2T_x$ MXenes and UiO-66 MOFs were used for this purpose. $Ti_3C_2T_x$ MXenes were synthesized via NH_4HF_2 and citric acid chemical etching. UiO-66 MOFs were synthesized through hydrothermal technique. $Ti_3C_2T_x$/UiO-66 composite was synthesized through an in-situ synthesis approach. Three $Ti_3C_2T_x$/UiO-66 composites were synthesized, based on different mass ratios, i.e., 1:1, 1:2 and 2:1 of $Ti_3C_2T_x$:UiO-66. Electrochemical testing was performed to evaluate HER performance of the synthesized electrocatalyst. The electrochemical testing results showed that the MX-2/MOF had lowest HER and OER potentials of 93 and 77 mV respectively. Moreover, the electrocatalyst had lowest Tafel slope of 86 $mVdec^{-1}$. The catalyst was highly stable and retained its activity even after 6h. Thus, $Ti_3C_2T_x$ MXenes/UiO-66 MOFs composites can serve for electrocatalytic H_2 production.

Keywords: MXenes, Electrocatalyst, H_2 production, Water splitting.

Table of Contents

List of Figures

List of Tables

Chapter 1:

Introduction

1.1 Background

The extinction of fossil fuels is giving rise to energy crisis around the world, since fossil fuels are major energy production source, there is need of new technologies for energy generation keeping the environmental safety in view. Hydrogen energy is the best alternative so far discovered. Hydrogen energy source is buildout of clean energy technologies. The abundant amount of hydrogen, its environmentally benign nature, and higher calorific values than new energy technologies make it promising energy source in sustainable energy development. The conventional H_2 production methods such as steam reforming produces CO_2 as a byproduct which ultimately causes global warming. A zero-carbon technology for H_2 generation is electrolysis of water, the method is environmentally safer however intense energy requirements make it undesirable. MXenes based catalysts can best serve for hydrogen (H_2) production. MXenes materials possess high metallic conductivity and hydrophilicity, which play fundamental role in catalytic applications. MXenes are superior candidate for catalytic applications than other 2D nanomaterials such as metal organic frameworks (MOFs), graphene and transition metal dichalcogenides (TMDs). The higher catalytic activity of MXenes is due to their high metallic conductivity, hydrophobic surfaces and abundant reactive sites. MXenes act as carbon support to provide channels for effective conduction of electrons but prevents the corrosion of carbon support up to notable catalytic cycles [1, 2].

The majority of H_2 production relies on the reforming of fossil reserves, generating a large amount of carbon dioxide. Currently, steam reforming is the dominant way for the hydrogen production in industry, which produces the commercial hydrogen at about 95 % of the world production. In the reforming process, steam reacts with methane at high temperature and pressure on nickel catalyst. However, the process releases a huge amount of CO_2 that is 8 times higher than that of hydrogen produced leading to ever-increased greenhouse effect. Presently, 96% of the industrial hydrogen production is done through fossil-fuel based technologies, The remaining 4% of the industrial hydrogen production is carried out by electrocatalytic splitting of water. H_2 produced by electrocatalytic water-splitting is extremely pure (>99%) and yields no toxic by-products or greenhouse emissions. A major advantage of electrocatalytic water-splitting is that it can be

coupled to intermittent energy sources (solar, wind, etc.) and utilize the excess energy to produce storable hydrogen. The stored hydrogen can be used for on-site applications or transported to distant locations with appropriate handling [3].
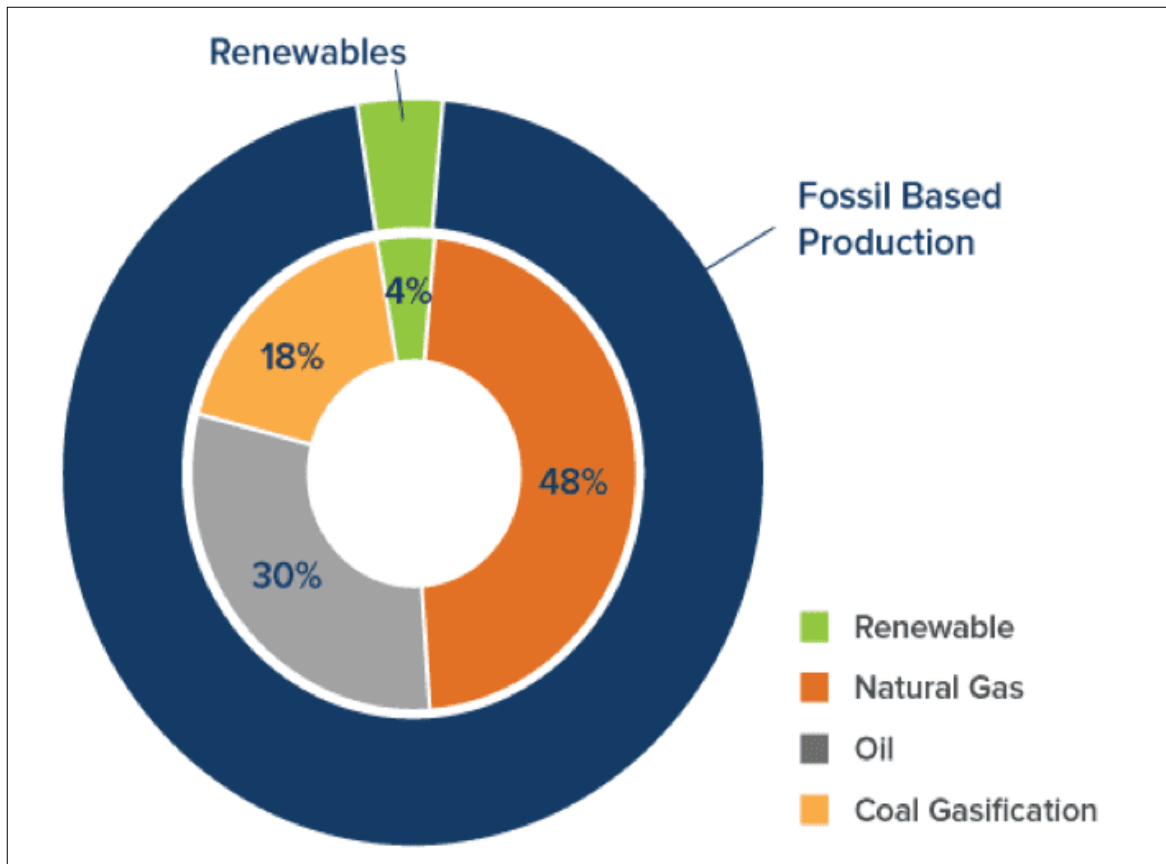
Figure 1.1: Worlds energy production sources.

1.2 Importance of H_2 Energy

Molecular hydrogen (H_2) is considered to be the most promising candidate for replacing fossil fuels because of its high energy density and zero carbon emission. As a result, clean ways for the production of hydrogen are highly expected. Hydrogen as energy has attracted much attention due to its rich resources and high calorific value among new energy technologies.

Water electrolysis can produce a high purity H_2 for energy purposes. Since water is present in abundant amount. The produced hydrogen gas can also be combined with carbon dioxide emitted from burnt coals and plastics, to release harmless natural gas or as source of agrofertilizers. Use gas grid for heating and cooking purposes. H_2 production through cleaner production technologies like water electrolysis and steam methane reforming with carbon capture storage, can develop

commercial viability into mass markets. Large scale H_2 storage contributes to achieving zero-carbon footprint in various fields, including industry, transportation, buildings and fuel cells.

H_2 is widely used in industry, about 70 million tons of H_2 was consumed annually by industries in 2019, in its pure form. It is expected that H_2 production market for industrial uses to grow to \$155 billion in 2022 [4, 5]. H_2 is critical reactant in chemical process industries, such as ammonia production and fertilizers. Ammonia is produced by Haber-Bosch process through reaction, i.e., $H_2 + N_2 \leftrightarrow 2NH_3$. Oil refineries are largest consumers of H_2, which is produced by steam reforming on-site, as captive H_2, which contributes to 33 % of world's H_2 production. H_2 is used for processing of crude oil to refined fuels [6].

Another advantage is hydrogen's energy density. Diesel has an energy density of 45.5 megajoules per kilogram (MJ/kg), slightly lower than gasoline, which has an energy density of 45.8 MJ/kg. By contrast, hydrogen has an energy density of approximately 120 MJ/kg, almost three times more than diesel or gasoline. In electrical terms, the energy density of hydrogen is equal to 33.6 kWh of usable energy per kg, versus diesel which only holds about 12–14 kWh per kg. What this really means is that 1 kg of hydrogen, used in a fuel cell to power an electric motor, contains approximately the same energy as a gallon of diesel. Taking this into consideration, Nikola claims its vehicles can get between 12 and 15 mpg equivalent, well above the national average for a diesel truck, which is around 6.4 mpg. IEA analysis finds that the cost of producing hydrogen could fall 30% by 2030 as a result of declining costs of renewables and the scaling up of hydrogen production [7].
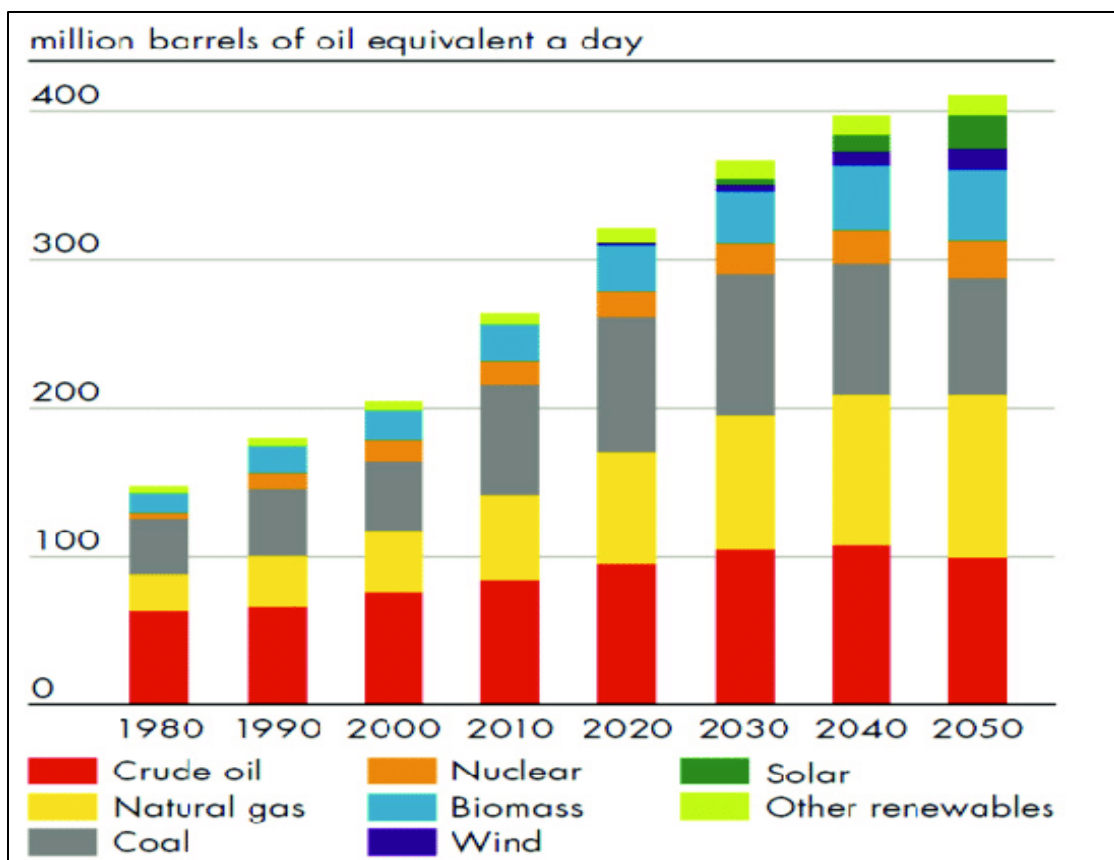
Figure 1.2: Energy production sources in timeline 1980-2050.

1.3 Hydrogen Evolution Reaction

Hydrogen evolution reaction (HER), the reductive half reaction of water splitting, provides a clean and renewable way to produce hydrogen at the cost of electric energy. Obviously, developing highly efficient HER electrocatalysts to minimize the overpotential and facilitate the reaction kinetics is one of the prerequisites to realize industrial electrocatalytic hydrogen production in large-scale.

1.3.1 Electrocatalytic HER Mechanism

Hydrogen generation by water splitting through electrocatalysts is subject of interest for researchers due to minimum power consumption [8].

Electrocatalytic HER mechanism relies on adsorption and desorption of hydrogen on catalyst surface. The adsorbed hydrogen forms intermediate product H* (Volmer reaction). The hydrogen gas is released upon desorption of hydrogen (Tafel reaction or Heyrovsky reaction). The binding strength of H* on the electrocatalyst surface is defined in terms of Gibbs free energy, ΔG^*, which defines the difficulty of reaction initiation on catalyst. The ΔG^* value close to zero is desired for

hydrogen evolution, it indicates equilibrium between the adsorption and desorption process. The electrical driven hydrogen production contains hydrogen evolution reaction on the cathode which is a two-electron route reaction and the oxygen evolution reaction on anode, a four-electron route reaction. These reactions are expressed through a combined mechanism termed as Volmer–Heyrovsky or Volmer–Tafel mechanism [9, 10].

$$H_2O + e \rightarrow H_{ads} + OH^- \qquad (Volmer)$$

$$H_2O + H_{ads} + e \rightarrow H_2 + OH^- \qquad (Heyrovsky)$$

$$H_{ads} + H_{ads} + 2e \rightarrow H_2 \qquad (Tafel)$$
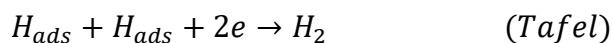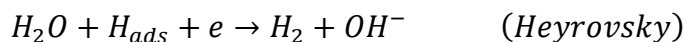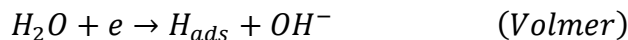
Since HER is based on adsorption/desorption of hydrogen, therefore it relies on electrochemical adsorption (Volmer) and desorption, followed by either electrochemical (Heyrovsky) or chemical (Tafel) step [11-14]. Volmer step includes hydrogen (H*) adsorption on active sites of electrocatalyst. The adsorbed hydrogen then combines either with a proton in vicinity electron in Heyrovsky step to yield hydrogen gas or proceed to Tafel step in which hydrogen atoms combine to form hydrogen molecule. ΔG* is critical factor in electrocatalysis for HER. An efficient catalyst requires ΔG* approaching to zero for a thermal -neutral reaction and a small Tafel slope for high charge transfer. Large values of ΔG* (positive or negative) hinders proton attraction and hydrogen release. [15-18]

In H* adsorption/desorption the interaction of H* with the active sites of catalyst significantly affect the catalytic activity of electrocatalyst. The d-band of noble metals conduct adsorption/desorption process by interacting with H*. The partially filled d-orbital of transition metals (such as Co, Ni, Fe, W and Mo) interacts with 1s orbital of H by providing active sites for H adsorption. However, the strong binding force of transition metals with H make desorption the rate-determining step in HER. The transition metals can be alloyed to change their d-band state and modulate the binding forces to improve the catalytic activity of transition metals. Introduction of small radius atoms into lattice structure causes d-band contraction which move up the d-band center towards Fermi energy level. The interaction between transition metal and H* is weaken, resulting in improved catalytic process by faster hydrogen desorption. The transition metal carbides and nitrides are suitable candidates for this d-band adjustment for HER. MXenes structure make them a promising electrocatalyst for HER, transition metals on outer layer provide electrocatalytic potential simultaneously the C/N atoms in middle layer or and the surface terminations monitor their electronic structures. [19-23]
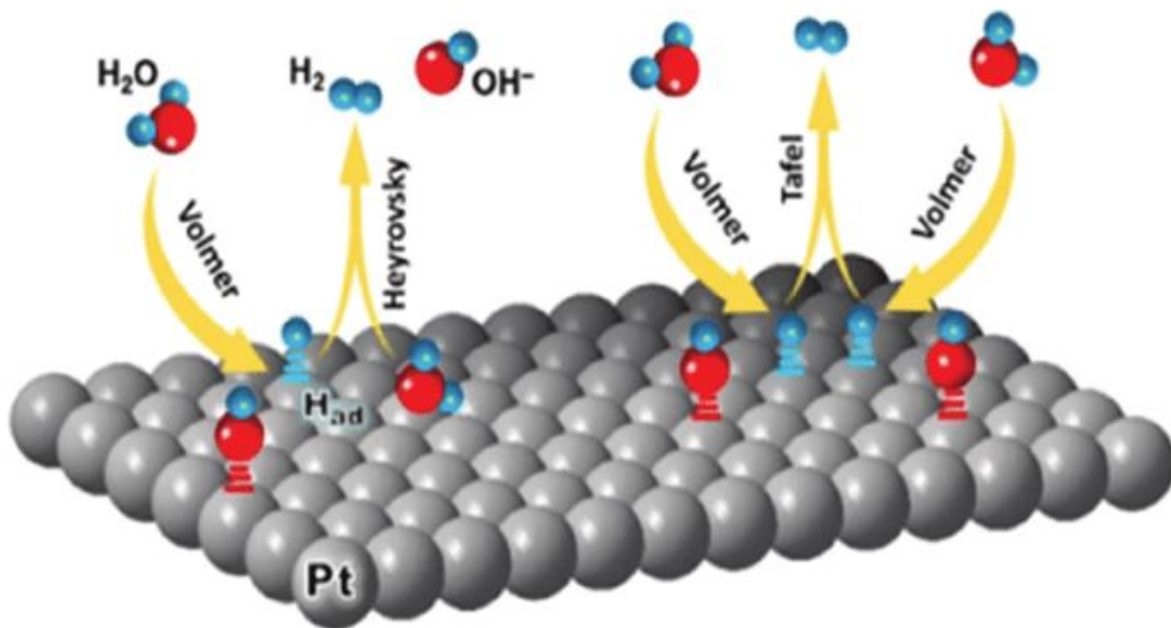
Figure 1.3: HER mechanism.

1.4 MXenes

Acquisition of two-dimensional (2D) nanomaterials in diverse applications paved a way forward for researchers to explore them. MXenes is one of such 2D materials, they are carbides and nitrides of transition metals or sometimes transition metal carbonitrides. The first MXenes was discovered in 2011 at Drexel University, since then more than 30 MXenes' composition have been published [24].

MXenes are conventionally synthesized by chemical etching of precursor known as MAX phase. Max phase is polycrystalline structure of carbides and nitrides. MAX phase is expressed as $M_{n+1}AX_n$ (n=1-3), where M symbolize early d-block transition metals, A belongs to group IIIA or IVA element of periodic table and X represents carbon (C) or nitrogen (N). A layer of MAX phase is removed to give 2D flakes of MXenes through etching. The A general representation of MXenes is $M_{n+1}X_nT_x$, where T_x shows functional groups such as fluorine (F)/chlorine [4], oxygen (O) or hydroxyl (-OH) atoms bonded on outer layer of transition metals (M) [24, 25].

Most MXenes are synthesized through chemical etching. Hydrofluoric acid (HF) was the first etchant used in this respect. $Ti_3C_2T_x$ was the first MXene was synthesized etching of Aluminum (Al) layer from the Ti_3AlC_2 MAX phase, with hydrofluoric acid (HF) as etchant. HF being hazardous to environment was replaced by safer etchants which causes in-situ formation of HF, such as fluoride salts and strong acid (LiF, NH_4F, KF and NaF with HCl) and bifluoride salts

6

(NH_4HF_2, $NaHF_2$ and KHF_2). The toxic nature of HF is major drawback in HF-based MXenes synthesis. Therefore, new routes such electrochemical etching, ionic liquid-based etching, chemical vapor deposition and deep eutectic solvent are devised for HF-free synthesis of MXenes. MXenes-based materials are also contributing towards emerging energy production technologies. $Ti_3C_2T_x$ MXenes
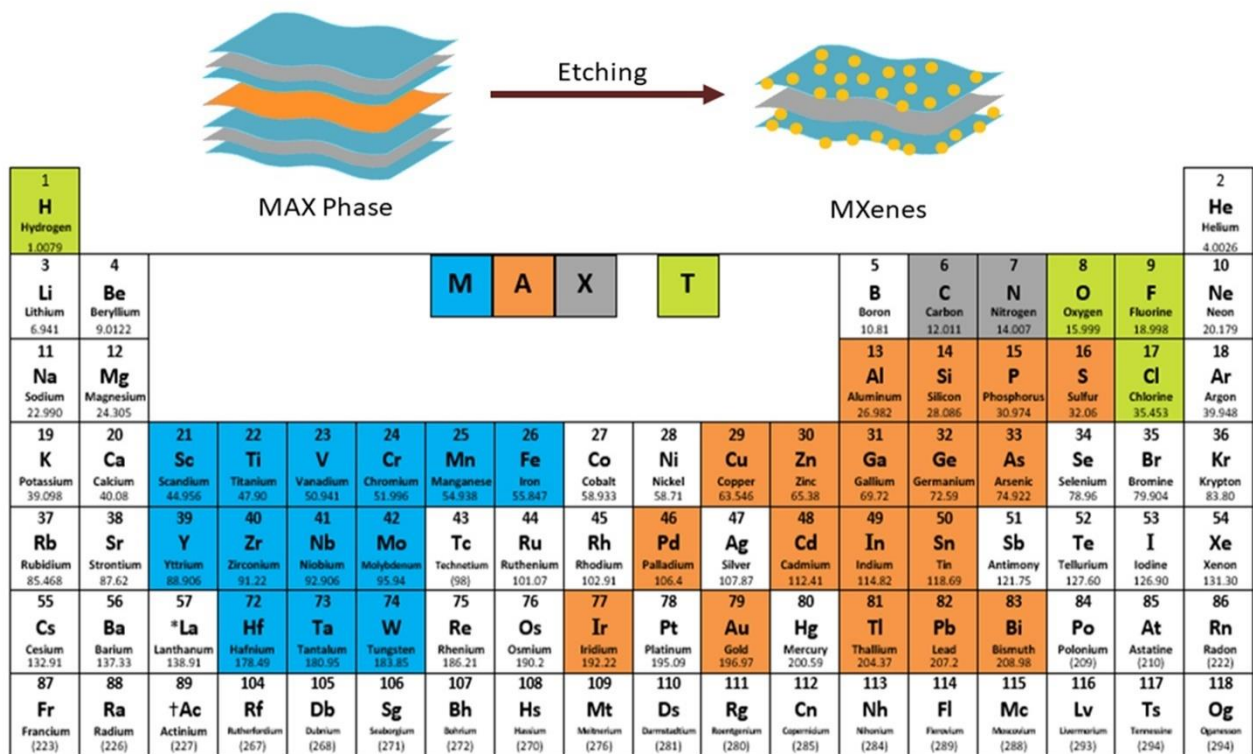
Figure 1.4: MAX phase and MXenes structure.

1.5 MOFs

MOFs are promising materials for electrocatalytic applications due to their high surface area and active centers which include transition metal sites and functional groups [26].

1.5.1 UiO-66 MOFs

The poor stability of MOFs derived from the reversible nature of coordination bonds is commonly regarded as the major drawback for their practical applications in most research fields. Post synthesis modifications enhance stability against moisture, after thermal modification and formation of an amorphous carbon coating on the MOF particle surfaces. improved stability of the MOFs after post-treatment is always expensive. Much research has been invested to directly construct MOFs with inherent stability in structure and composition. The discovery of UiO-66.

The structure of UiO-66 exhibits unprecedented stability, especially hydrothermal stability beyond most reported MOFs.

One key feature of Zr-MOFs is the high oxidation state of Zr compared with M(I), M(II), and M(III)-based MOFs (M stands for metal elements). Due to high charge density and bond polarization, there is a strong affinity between Zr and carboxylate O atoms in most carboxylate-based Zr-MOFs. Zr ions and carboxylate ligands are considered hard acid and hard base, respectively, and their coordination bonds are strong. As a result, most Zr-MOFs are stable in organic solvents and water, and even tolerable to acidic aqueous solution. Also electrolyte used in electrochemical testing is acid to MOFs can operate in acidic conditions. [27]

UiO-66 is a Zr-based MOF having exceptional hydrothermal stability and is a model compound for diverse post-synthesis organic functionalization. Zirconium is highly resistant to corrosion and has a high affinity for hard oxygen donor ligands. As anticipated from the strong Zr-carboxylate bonding, UiO-66 shows high chemical and thermal stability. UiO-66 is stable in polar protic solvents including water and alcohols. The crystallinity of UiO-66 was found to be retained even after treatment with aqueous HCl (pH=1) or aqueous NaOH (pH=14). Zirconium is widely distributed in nature and is found in all biological systems. The rich content and low toxicity of Zr further favor the development and application of Zr-MOFs.

1.6 MXenes/MOFs Composites

MXenes/MOFs composites are a type of hybrid material composed of two different classes of materials: two-dimensional transition metal carbides, nitrides, or carbonitrides (MXenes), and metal-organic frameworks (MOFs). These composites combine the unique properties of both MXenes and MOFs and offer enhanced properties and performance for various applications, such as gas separation, energy storage, and catalysis.

Even though MOFs possess high surface area and large number of active sites, The major restriction in their application for catalysis is poor stability and low thermal and electrical conductivity. MOFs are not stable against moisture, they have inferior electrocatalytic activity due to low electrical conductivity. This issue can be mitigated by hybridizing MOFs with other materials, such as 2D materials. MXenes are emerging 2D materials owing to rich surface chemistry and stimulating electrochemical properties. MXenes have been reinforced with MOFs to boost up stability, electrical conductivity and catalytic activity of MOFs. Moreover, this composites formation prevents the oxidation of MXenes. MXenes provide structural stability and

charge transport medium to active catalyst sites. MXenes suffer from oxidation and restaking which limit their surface area and electrochemical properties. MXenes/MOFs composites unites the unique properties of both the MXenes and MOFs resulting in enhanced surface area, electrochemical properties and stability.

1.6.1   Synthesis of MXenes/MOFs Composites

Here is a general synthesis process for MXenes/MOFs composites:

Synthesis of MXenes: The first step is to synthesize MXenes following the steps mentioned earlier, i.e., etching the precursor MAX phase with a strong acid to obtain MXenes.

Synthesis of MOFs: The second step is to synthesize MOFs using various synthesis methods, such as solvothermal, microwave, or electrochemical synthesis.

Preparation of MXenes/MOFs composites: The MXenes/MOFs composites can be prepared by various methods, including direct mixing, in situ growth, or layer-by-layer assembly. Direct mixing involves the physical mixing of MXenes and MOFs in a solvent followed by drying and annealing to form a composite. In situ growth involves the growth of MOFs on the surface of MXenes by introducing metal ions and organic ligands in the MXene suspension. Layer-by-layer assembly involves the sequential deposition of MXenes and MOFs on a substrate to form a thin film.

The resulting MXenes/MOFs composites exhibit enhanced properties compared to their individual components, such as increased surface area, improved stability, and synergistic effects in catalytic reactions. These composites have great potential for various applications, including gas separation, energy storage, and catalysis.
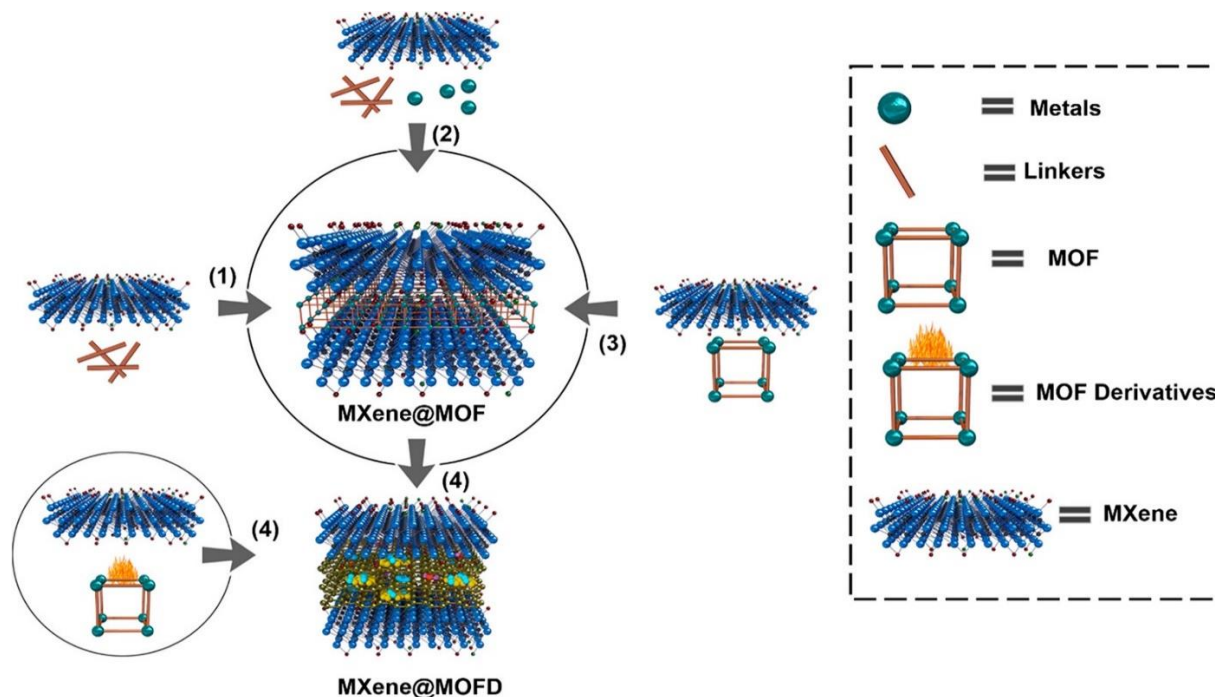
Figure 1.5: MXenes/MOFs composites' structure.

1.7 Research Problem

H$_2$ production through water electrolysis can contribute to achieving zero-carbon footprint. Developing highly efficient HER electrocatalysts is a prerequisite for electrocatalytic H$_2$ production. The application of MXenes for electrocatalytic H$_2$ production is an important development. Our research aims at synthesis of Ti$_3$C$_2$T$_x$/UiO-66 MOFs composite and its application in electrocatalytic HER.

1.8 Research Objectives

1. Synthesis and characterization of Ti$_3$C$_2$T$_x$/MOFs electrocatalyst.
2. Application of Ti$_3$C$_2$T$_x$/MOFs electrocatalyst for optimum H$_2$ production.

Chapter 2:

Literature Review

MOFs generally have lower conductivity therefore they are incorporated with other materials to give a composite with enhanced conductivity. MXenes and MOFs composite is one such example which unites the properties of MXenes and MOFs to give electrocatalyst for enhanced HER.

2.1 MXenes/MOFs Composites Synthesis

2.1.1 In-Situ Synthesis Method

In situ technique was adopted widely for synthesis of nano-heterostructures. Zhao et al. synthesized a composite of $Ti_3C_2T_x$ MXenes with CoBDC MOFs by in situ synthesis method. Co metal salt, 1,4-BDC were reacted with $Ti_3C_2T_x$ MXenes in test tube. By this method CoBDC was coated on MXenes sheets' surfaces. The composite showed enhanced electrocatalytic performance [28].

The Ti_3C_2-QD/Ni-FOM nanosheets were synthesized by Qin and co-workers. In-situ strategy was adopted for the synthesis. The nanosheets were prepared by ultrasonication. $NiCl_2.6H_2O$ and BDC were dissolved in mixture of DMF, ethanol and deionized mixture, under ultrasonication. The TEA and Ti_3C_2-QD were injected into the solution under continuous ultrasonication. The product was washed with ethanol and dried. The synthesized Ti_3C_2-QD/Ni-FOM photocatalyst was used for N_2 fixation [29].

In-situ synthesis of dual metal MOF and MXenes based materials was carried out. The Co-Zn-ZIF MOF was hybridized with $Ti_3C_2T_x$ MXenes by mixing of cobalt and zinc metal salts, $Ti_3C_2T_x$ MXenes and 2-methylimidazole. The synthesized Co-Zn-ZIF/ $Ti_3C_2T_x$ composite was subjected to calcination under inert environment. During calcination Zn was evaporated and CoO_x-N-C/TiO_2C was obtained [30].

A $Ti_3C_2T_x$ MXenes supported CoNi-ZIF-67 composite was synthesized through in-situ growth of CoNi-ZIF-67 on $Ti_3C_2T_x$, by coprecipitation reaction. The CoNi-ZIF-67/$Ti_3C_2T_x$ composite was synthesized by mixing solution of methanol containing $Ti_3C_2T_x$, $Co(NO_3)_2.6H_2O$ and $Ni(NO_3)_2.6H_2O$, with solution of methanol containing 2-methylimidazole. Hexadecyl trimethyl ammonium bromide (CTAB) was added to the mixed solution followed by continuous mixing at room temperature for 8 h. Final precipitates were obtained by washing with methanol and water, through centrifugation, and dried at 60 ℃, under vacuum. The CoNi-ZIF-67/$Ti_3C_2T_x$ composite

was used as electrocatalyst for OER, which showed enhanced performance than pristine $Ti_3C_2T_x$ MXenes and CoNi-ZIF-67 [31].
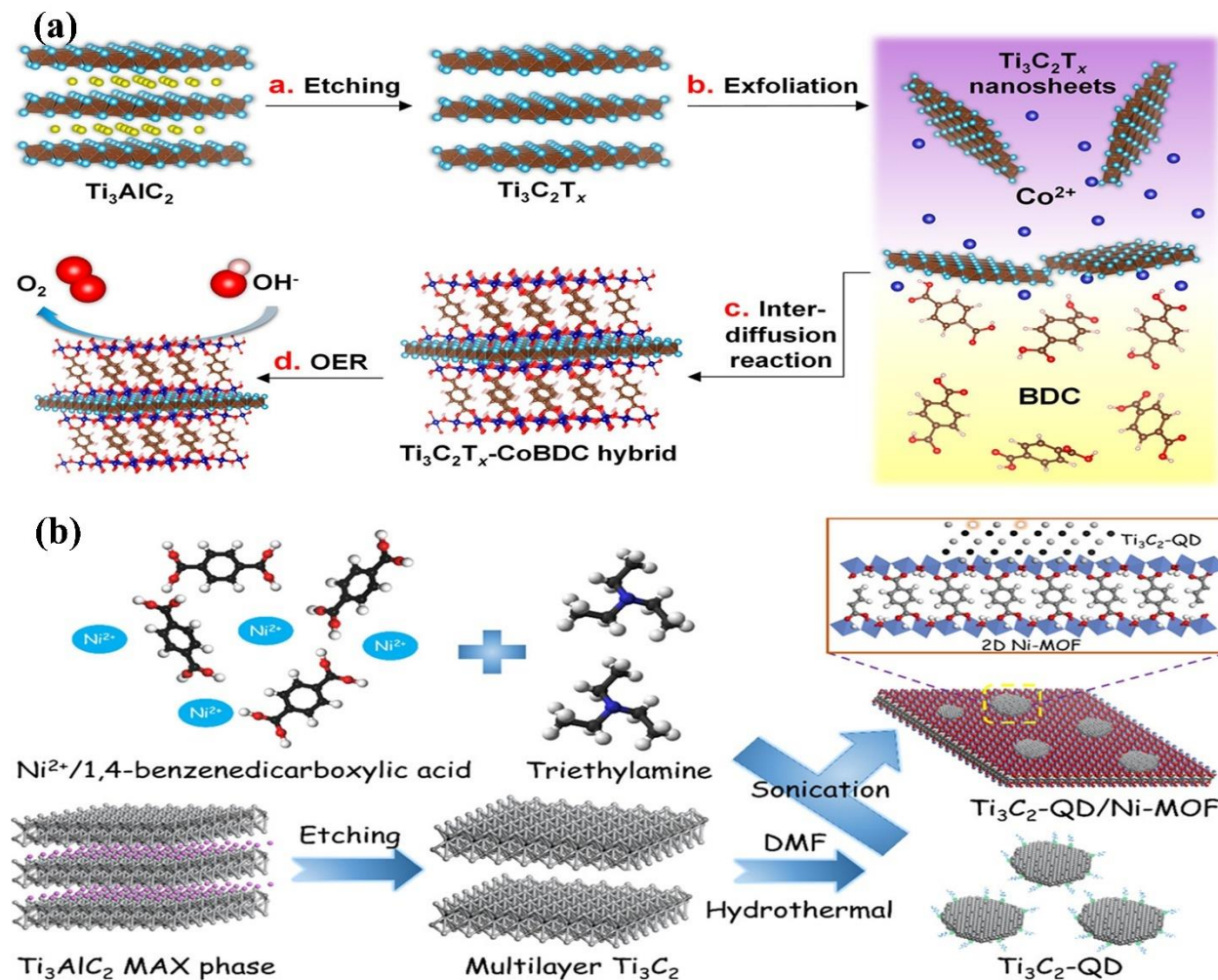
Figure 2.1: In-situ MXenes/MOFs synthesis method.

2.1.2 Mixing Method

MXenes/MOFs composites can be synthesized by facile mixing of the two components, followed by treatment of resulting mixture under suitable conditions. The binding forces in this case are weak wander forces and hydrogen bonding. Zhao et al synthesized a hydrogen-bonded composite of metal−porphyrin frameworks (MPFs) and $Ti_3C_2T_x$ MXenes. The two components were mixed and a stacked MPFs/ $Ti_3C_2T_x$ MXenes was obtained after vacuum filtration. The synthesized composite possessed large interlayer spacing [32].
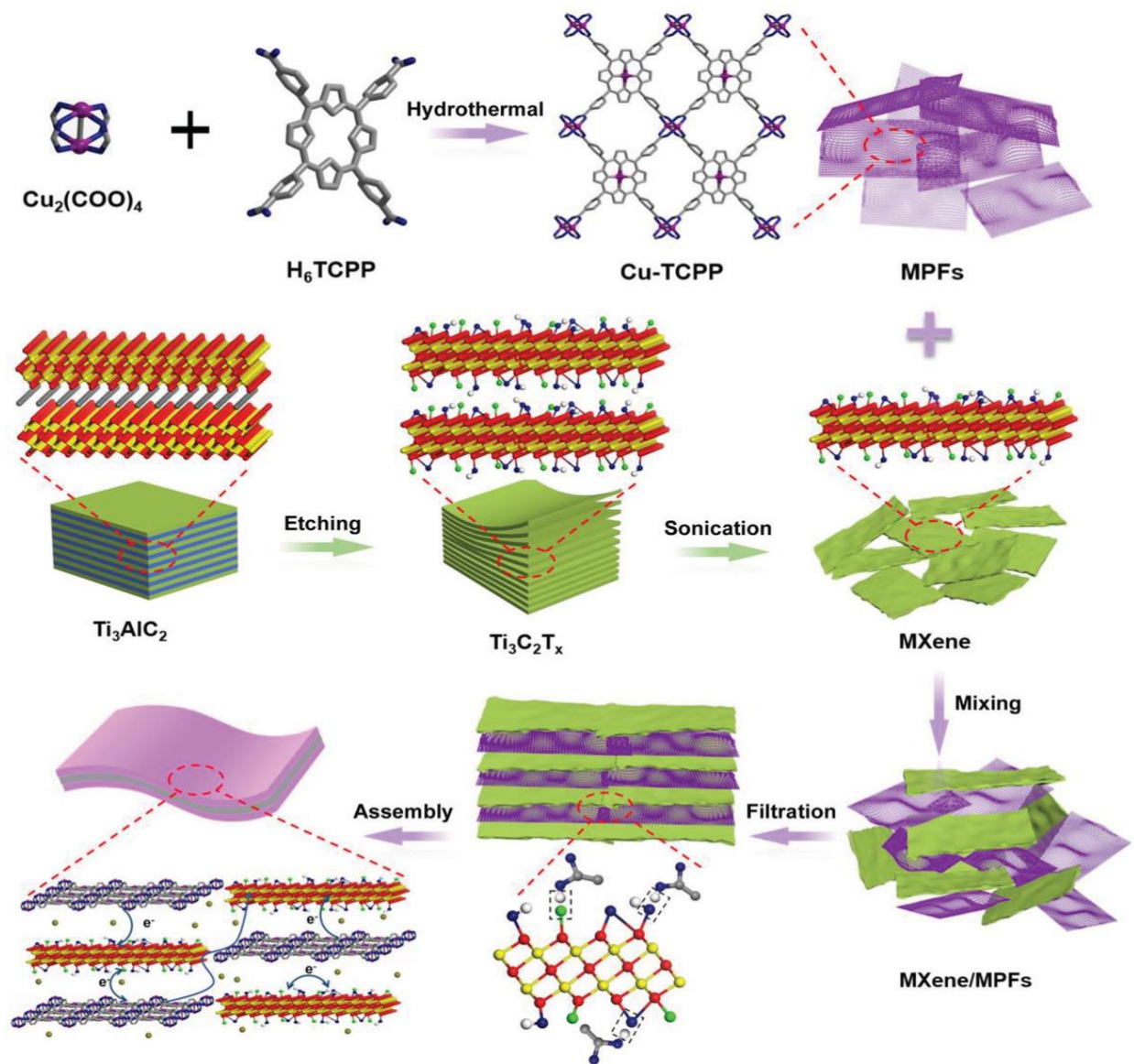
Figure 2.2: Mixing method for synthesis of MXenes/MOFs composite

2.2 $Ti_3C_2T_x$ MXenes-based Electrocatalysts for H_2 Generation

The nanoparticles are emerging candidates for HER catalysts due to their immense surface energy and surface area. Beside their high catalytic activity, they are also inclined for favor catalytic deactivation. MXenes possess high specific surface area and potent the electrical conductivity of nanoparticles when used as substrate to fabricate nano-hybrids [33]. Pt is the most efficient noble metal electrocatalyst for HER. The Pt/C catalyst is used commercially in HER applications. It is composed of 5-20% Pt loaded on carbon black. Despite of its efficiency the poisoning effect and high cost of Pt/C catalyst are constraints in their practical applications. Therefore, it is essential to develop an efficient and cost effective HER catalyst. Pt can be alloyed with non-noble metals to

devise an electrocatalyst with enhanced intrinsic activity and reduced Pt amount. The Pt-alloyed nanoparticles are thermodynamically stable which aids in catalytic regeneration in industrial applications. The controlled particle sizes in Pt-based alloy NPs promote HER activity by increasing number of active sites and enhancing reactivity of these sites. Recently the MXenes-based electrocatalyst gathered attention because these hybrid structures enhance the electrochemical activity. Pt nanoparticles alloyed with $Ti_3C_2T_x$ with minimum Pt content exhibit improved HER activity. The $Pt_3Ti/Ti_3C_2T_x$ composite formed of Pt_3Ti intermetallic nanoparticles (iNPs) on $Ti_3C_2T_x$ MXene is an efficient electrocatalyst for HER. [34-41]

Wu et al. synthesized the electrocatalyst through in-situ co-reduction. The synthesis was caried out at different temperatures to get the optimum HER electrocatalyst. The optimum H* adsorption strength of catalyst was observed for reduction temperature of 550 ℃. The catalyst showed small Tafel slope, higher mass, lower overpotential, higher stability and greater specific activity than a commercial Pt/C catalyst. Pt precursors were loaded on HF synthesized $Ti_3C_2T_x$ MXenes via incipient wetness impregnation (IWI). Then reduction was carried under H_2/Ar atmosphere at 550 ℃ to obtain $Pt/Ti_3C_2T_x$ electrocatalyst. HER performance of the electrocatalyst was evaluated using three-electrode system with a hydrogen cell having two compartments. The $Pt/Ti_3C_2T_x$ electrocatalyst showed very small overpotential (η) at 10 mA of 32.7 mV and 40 mA at 60.8 mV. The overpotential at 10 mA of $Pt/Ti_3C_2T_x$ was 23 mV which is lower than overpotential of Pt/C catalyst with same Pt amount. Mass activity of $Pt/Ti_3C_2T_x$ at 50 mV overpotential was 1.3 mA μg^{-1}, it was 3.3 times greater than that of Pt/C catalyst. The mass activity of $Pt/Ti_3C_2T_x$ (2.65 mA μg^{-1}) was also observed to be 4.4 times higher than for Pt/C catalyst (0.6 mA μg^{-1}). The $Pt/Ti_3C_2T_x$ exhibited excellent stability, an increase in overpotential of 2.5 mV was noticed in 2000th cycle. [42]

The 2D hierarchical MoS_2/Ti_3C_2-MXene@C nanohybrid was produced to determine the performance of these MXenes-based nanohybrids in electrocatalytic HER. MXenes coated with carbon layer prevents degradation and oxidation of MXenes structure. Ti_3C_2 MXene nanosheets were synthesized through exfoliation of Ti_3AlC_2 MAX phase via LiF/HCl etchant. The negatively charged oxygen and fluoride ions on MXenes surface electrostatically adsorb metal ions from ammonium molybdate tetrahydrate (AMT) to form MoS_2 nanoplates through reaction with thiourea and glucose. The MoS_2/Ti_3C_2-MXene@C nanohybrid tested for HER application showed that the electrocatalyst required small overpotential of 135 mV for 10 mA cm^{-2} current density.

Tafel slope of 45 mV dec^{-1} was obtained. By extrapolation of Tafel slope it was determined that the electrocatalyst had current density of 29 µA cm^{-2} which was higher over that of Pt/C (11 µA cm^{-2}). The MoS$_2$/Ti$_3$C$_2$-MXene@C electrocatalyst exhibited good stability. Long-term cyclic volumetric cycling conducted on electrodes in 0.5 H$_2$SO$_4$ at scan rate of 50 mV s^{-1}, the polarization curves showed negligible shift after 2000 cycles. [43]

The MoS$_2$/Ti$_3$C$_2$ hybrid electrocatalyst synthesized through microwave method showed an overpotential of 110 mV at 10 mA cm^{-2}, lower than bare MoS$_2$ which was 169 mV at same current density. [44] Similarly, MoS$_2$/Nb$_2$CT$_x$ synthesized through hydrothermal route exhibited an overpotential of 127 mV at 10 mA cm^{-2}. The Tafel slope of 56.3 mV dec^{-1} was obtained in acidic media. The enhanced performance of these hybrid electrocatalysts was ascribed by MXenes ability to easily transfer electrons to MoS$_2$ catalyst and reducing resistance to charge transfer. [45]

The transition metal [1] adsorbed V$_2$CO$_2$ MXene was analyzed as electrocatalyst for HER, with different TMs. The TM- promoted V$_2$CO$_2$ was investigated for cobalt (Co), iron (Fe) and nickel (Ni) to determine HER activity of MXene based electrocatalysts. The ΔG* for Ni-V$_2$CO$_2$, Fe-V$_2$CO$_2$ and Co-V$_2$CO$_2$ were observed to be -0.01, -0.04 and -0.03 eV respectively, smaller than ΔG* of Pt surface (0.09 eV). Thus these TM- V$_2$CO$_2$ indicated excellent HER catalytic activity. [46]

MXenes nanosheets of double transition metal (Mo$_2$TiC$_2$T$_x$) provide plenty of Mo vacancies which served as anchoring sites for single Pt atoms. The Mo$_2$TiC$_2$T$_x$ -Pt$_{SA}$ catalyst was synthesized through electrochemical exfoliation process, during which the Pt atoms immobilize on Mo vacancies. Pt atoms formed Pt-C bonds with the C atoms on MXenes to stabilize. The HER activity of Mo$_2$TiC$_2$T$_x$ -Pt$_{SA}$ catalyst was examined three electrode system with graphite counter electrode in 0.5M H$_2$SO$_4$ electrolyte. The Mo$_2$TiC$_2$T$_x$ -Pt$_{SA}$ showed that overpotential of 30, 77 and 104 mV were required to reach 10, 100 and 200 mA cm^{-2} current densities. The catalyst exhibited Pt-like kinetics with Tafel slope of 30 mV dec^{-1}, affirming rapid HER activity. The catalyst had mass activity of 8.3 A g^{-1} for HER activity which was 39.5 times higher than that of Pt/C commercial HER catalyst. The catalyst exhibited excellent stability beyond 10,000 HER cycles. [47]

The Pt$_x$Ni ultrathin nanowires (NWs) formed composite with Ti$_3$C$_2$ through in situ NWs grown on MXenes nanosheets with varying Pt compositions (x = 1.4, 3.21 and 5.67). The Pt$_x$Ni/Ti$_3$C$_2$ electrocatalysts exhibited exceptional HER performance in acidic and alkaline solutions. By using three electrode setup the electrocatalytic performance of Pt$_{1.4}$Ni/Ti$_3$C$_2$, Pt$_{3.21}$Ni/Ti$_3$C$_2$ and

$Pt_{5.67}Ni/Ti_3C_2$ was evaluated. The role of Ti_3C_2 MXene in HER was demonstrated by comparison with free standing $Pt_{3.21}Ni$ NWs. The $Pt_{3.21}Ni/Ti_3C_2$ showed smallest Tafel slope amongst all others which was 13.3 mv dec^{-1}, while $Pt_{1.4}Ni/Ti_3C_2$, $Pt_{5.67}Ni/Ti_3C_2$ and $Pt_{3.21}Ni$ had 27.7, 33.3 and 34.5 mV dec^{-1} respectively. This was due to ΔG^* of $Pt_{3.21}Ni/Ti_3C_2$ (-0.03 eV) was very close to optimal value. While the other samples; $Pt_{1.4}Ni/Ti_3C_2$, $Pt_{5.67}Ni/Ti_3C_2$ and $Pt_{3.21}Ni$ NWs had ΔG^* values of -0.08, -0.13 and -0.15 eV. Thus, coupling of Pt_xNi (x=3.21) and Ti_3C_2 nanosheets resulted in enhanced performance HER electrocatalyst with very small ΔG^*. [48]

2.3 MXenes/MOFs Electrocatalysts

The $Ti_3C_2T_x$-CoBDC synthesized via in situ method showed OER overpotential of 164 mV at 10 mA cm^{-2} current density. The Tafel slope of the catalyst was 48.2 mV decade^{-1}, which was lower than CoBDC (48.8 mV decade^{-1}) and pristine $Ti_3C_2T_x$ MXenes (187.1 mV decade^{-1}) [28].

A novel approach for synthesis of Ni-Co-mixed metal sulfide/$Ti_3C_2T_x$ MXenes composite was adopted, to device electrocatalysts. It could benefit from unique structure and strong interfacial interaction between NiCoS and $Ti_3C_2T_x$ MXenes sheets. ZIF-67-MOF derivative was hybridized with $Ti_3C_2T_x$ MXenes through in-situ nucleation and conversion of ZIF-67 MOF to porous Ni-CO-mixed metal sulfide on $Ti_3C_2T_x$ MXenes nanosheets. The NiCoS/$Ti_3C_2T_x$ showed OER overpotential of 365 mV at current density of 10 mA cm^{-2} [49].

CoZn-ZIF/ $Ti_3C_2T_x$ composite was modified to CoO_x-N-C/ Ti_3O_2C composite, for electrocatalytic applications. Cobalt species, derived from CoZn-based MOF was combined with carbon nanotubes and loaded onto $Ti_3C_2T_x$ MXenes. The CoO_x-N-C/ Ti_3O_2C composite was used as electrocatalyst for water splitting. It showed that 10 mA cm^{-2} current density was achieved at 145 mV [50].

CoNi-ZIF-67/$Ti_3C_2T_x$ composite synthesized via in-situ approach was applied for electrocatalytic OER and showed better OER activity than the components i.e., CoNi-ZIF-67 and $Ti_3C_2T_x$ MXenes. $Ti_3C_2T_x$ MXenes showed no OER activity, CoNi-ZIF-67 showed overpotential of 341 mV for current density 10 mA cm^{-2}, whereas the CoNi-ZIF-67/$Ti_3C_2T_x$ electrocatalyst achieved 10 mA cm^{-2} current density at an overpotential of 275 mV. Hence it was seen that the composite exbibit properties that hold best for an electrocatalyst, including high surface area, increased conductivity and porosity. The specific surface area of $Ti_3C_2T_x$ MXenes, CoNi-ZIF-67 and CoNi-ZIF-67/$Ti_3C_2T_x$ composite was 14.1, 202.9 and 1135.8 m^{-2}/g [31]. Therefore, it can be concluded that the MXenes/MOFs composites have enhanced properties. MXenes are when hybridized with

MOFs the unique properties of MOFs and MXenes combined to give enhanced properties, which can be useful for electrocatalytic applications.

Chapter 3:

Methodology

$Ti_3C_2T_x$ MXenes, UiO-66 MOF and $Ti_3C_2T_x$ MXene/UiO-66 MOF composites were synthesized. MX/MOF composites were synthesized with varying mass ratios of MXenes and MOF.

3.1   Synthesis of $Ti_3C_2T_x$ MXenes

3.1.1   Chemicals

- 27.4 g NH_4HF_2 (4.8M NH_4HF_2 solution)
- 50 g (1.3M) citric acid
- 4 g Ti_3AlC_2 MAX phase powder

3.1.2   Procedure

Etching

1. Weighted 27.4 g of NH_4HF_2 in beaker and dissolved it in 100 ml deionized water to 4.8 M solution.
2. Weighted 50 g citric acid in beaker and dissolved it in 200 ml deionized water.
3. Added both solutions to a plastic bottle.
4. Added 200 ml deionized water to the solution.
5. Placed the glass bottle on magnetic stirrer plate. Inserted Teflon magnetic stirrer in it.
6. Weighed 4 g Max phase.
7. Slowly added 4 g of MAX phase to it.
8. Loosely closed the lid of the bottle.
9. Allowed the reaction to proceed for 24 hr, at room temperature with stirring at 750 (1/min).

Centrifugation

10. Noted pH before centrifugation, it was 3.
11. Performed centrifugation 4 cycles at 4500 rpm for 30 min.
12. Noted pH after centrifugation. The pH was 5.

Intercalation

13. Added 4 ml TMAOH in beaker and added 200 ml deionized water in it.
14. Added synthesized MXenes in it.
15. Allowed stirring at 750 1/min at room temperature for 72 hr.
16. Checked pH after intercalation, it was 7.7.

Vacuum Filtration

17. Vacuum filtration was performed with membrane specifications 0.45 μm.

18. Vacuum filtration was continued, the MXenes was washed with 2-liter deionized water.

19. MXenes paste was formed after vacuum filtration.

Vacuum Drying

20. MXenes paste was dried in vacuum oven at 90 ℃ for 60 hr. The sample was named as MX.

Mass of Synthesized MXenes

Mass of petri dish = 46.004 g

Mass of petri dish containing dried MXenes = 49.598 g

Mass of MXenes synthesized = 49.298 - 46.004 = 3.594 g
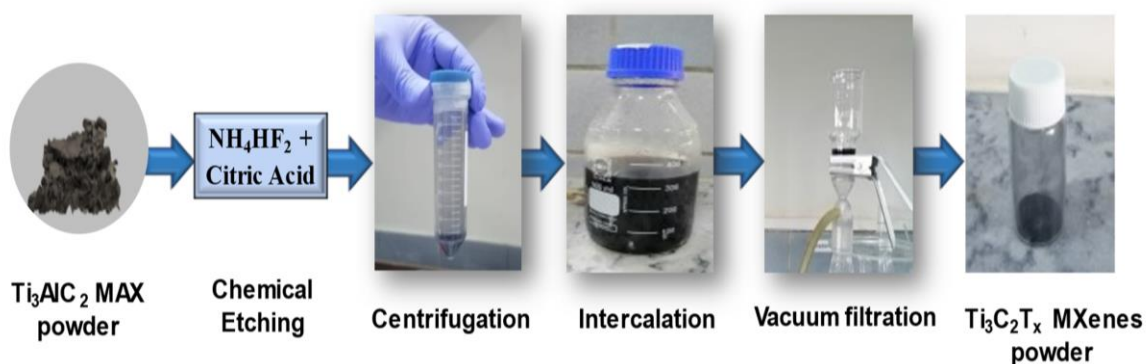
Figure 3.1: MXenes' synthesis method.

3.2   Synthesis of UiO-66 MOF

3.2.1   Chemicals

- 2.33 g of $ZrCl_4$ (0.5 M)
- 1.66 g of 1,4-benzenedicarboxylic acid (BDC) (0.5 M)
- 1,4-dimethylformamide (DMF)

3.2.2   Procedure

Reaction

1. Weighted 2.33 g of $ZrCl_4$.

2. The weighted $ZrCl_4$ was transferred to a beaker and DMF was added to make the volume of solution 20 ml.

3. Continuous stirring was allowed for 2 hr.

4. Weighted 1.66 g of BDC.

5. In a beaker weighted BDC was transferred and DMF was added to make the volume of solution 20 ml.

6. Continuous stirring was allowed for 2 hr.

7. Both solutions were mixed and placed the beaker in ultrasonication bath for 30 min.

8. The solution was transferred to Teflon lined stainless steel autoclave.

9. Reaction was carried out at 120 ℃ for 24 h.

Centrifugation

10. The product was washed with DMF and ethanol via centrifugation.

11. Three centrifugation cycles were performed at 4500 rpm for 15 mins.

12. A thick gel was obtained.

Drying

13. Gel was dried at 80 ℃ in oven for 48 hr.

14. The dried gel was grinded to form powder.

15. 2.29 g of powdered MOF gel was obtained. The sample was named as MOF.

ZrCl₄ + BDC+ DMF   Reaction 24 hr/ 120 ℃   Centrifugation   UiO-66 MOFs Powder
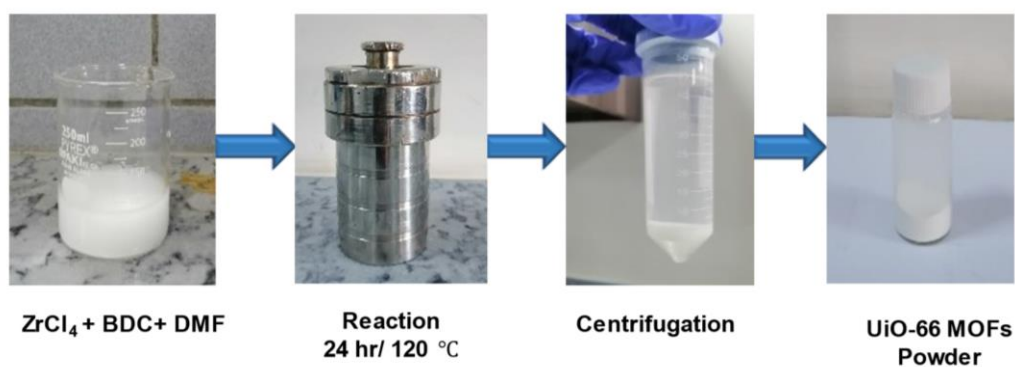
Figure 3.2: UiO-66 MOFs synthesis method.

3.3 Synthesis of MXenes/MOFs composites

3.3.1 Chemicals

- 0.466 g of ZrCl$_4$ (0.1 M)
- 0.332 g of 1,4-benzenedicarboxylic acid (BDC) (0.1 M)
- 1,4-dimethylformamide (DMF)
- 0.466 g of MXenes

3.3.2 Procedure

Reaction

1. Weighted 0.466 g of $ZrCl_4$.

2. The weighted $ZrCl_4$ was transferred to a beaker and DMF was added to make the volume of solution 20 ml.

3. Continuous stirring was allowed for 15 min.

4. Weighted 0.332 g of BDC.

5. Weighted BDC was transferred to beaker and DMF was added to make the volume of solution 20 ml.

6. Continuous stirring was allowed for 15 min.

7. Both solutions were mixed, and the final solution was labeled as "A".

8. 0.466 g of MXenes was dispersed in 10 ml DI water by 30 min sonication. The solution was labeled as "B".

9. Solutions A and B were mixed and stirred continuously for 2 hr.

10. Sonication was performed for 30 min.

11. The solution was transferred to Teflon lined stainless steel autoclave.

12. Reaction was carried in autoclave at 120 ℃ for 24 h.

Centrifugation

13. The product was washed with DMF and ethanol via centrifugation.

14. Three centrifugation cycles were performed at 4500 rpm for 15 mins.

15. A thick black gel was obtained.

Drying

16. Gel was dried at 80 ℃ in oven for 48 hr.

17. The dried gel was grinded to form powder.

18. 0.77 g of powdered MX/MOF gel was obtained.

19. Two more composites were synthesized in same manner, with 1:2 and 2:1 mass ratios of $Ti_3C_2T_x$ MXenes:UiO-66 MOF, labelled as MX-1/MOF and MX-2/MOF composites.
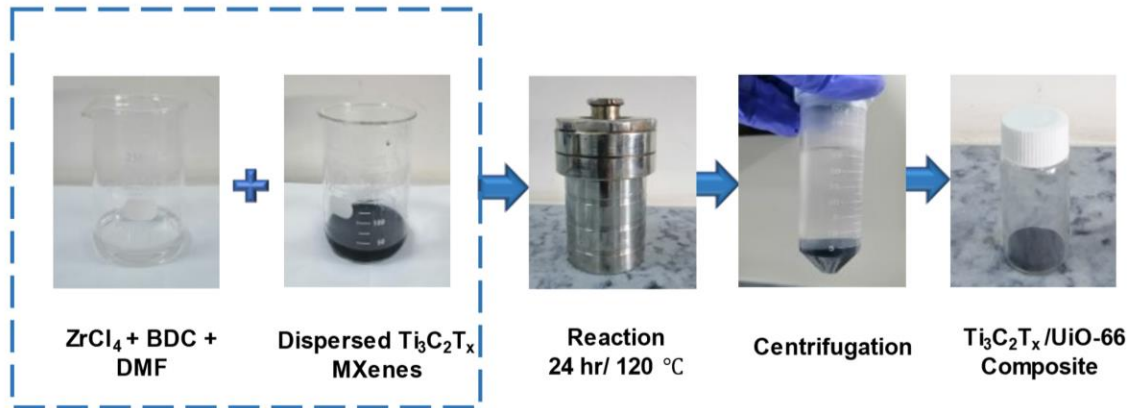
Figure 3.3: MXenes/UiO-66 composite synthesis method.

3.4 Materials Characterization

3.4.1 XRD

X-ray diffractometer analysis (XRD, STOE Germany) with Cu Kα irradiation was employed to determine crystal structure at 2θ ranging from 5 - 50°.

3.4.2 SEM

The structure and morphology of synthesized catalysts were characterized by Scanning Electron Microscopy (SEM, JEOL instrument JSM-6490A).

3.4.3 EDX

Composition analysis was performed on the SEM equipped with EDX. Surface area and pore structure were determined from N_2 sorption isotherms via Brunauer-Emmett-Teller method (Quantachrome TouchWin).

3.5 Electrodes Preparation

Electrode preparation contained ink formation, treatment of support material and deposition of ink on its surface.

Ink Formation

1. Ink was prepared by mixing 85 % of active catalyst, 10 % carbon black (conductive additive), 5 % Polyethylene difluoride (PVDF) as binder, and 0.4 ml 1-methyl-2-pyrrolidone (NMP) as solvent.

2. Mixture was sonicated for 3 h.

Support Material Treatment

3. Nickel foam served as conductive support material. 1×1 cm^2 Ni foam was cut.

4. It was treated by 30 min sonication in 2M HCL and ethanol each.

5. It was dried at 60 °C for 1 h.

Ink Deposition

6. The prepared ink was deposited on treated Ni foam to form electrode.

7. Electrode was dried at 80 °C for 24 h.

8. Five electrodes were prepared: MX, MOFs, MX/MOF, MX-1/MOF and MX-2/MOF by following the same procedure.

3.6 Electrochemical Testing

Electrochemical measurements were performed on three electrode system (Gamry Potentiostat) in 1M KOH aqueous electrolyte. Working electrode composed of catalyst deposited on Ni foam, Pt wire was used as counter electrode and Ag/AgCl as reference electrode.

CV measurements were performed from 0.0 – 0.6 V at scan rates of 50 and 100 mV s^{-1}. The OER activities of samples were examined through linear sweep voltammetry (LSV) in potential range from 0.0 – 1.5 V at scan rate of 10 mv s^{-1}. Electrochemical impedance spectroscopy (EIS) measurements were performed in frequency range of 1 to 100 kHz. Stability of catalyst was determined by chronopotentiometry for 6 h.

Chapter 4:

Results

The synthesized materials were characterized using XRD, SEM, EDX and BET. XRD determined the crystal structure and particle size. SEM and EXD were used to determine surface morphology and elemental composition. Through BET surface area of electrocatalysts was evaluated. Electrochemical testing was performed to evaluate HER and OER overpotentials, CV curves, electrochemical resistances and stability of electrocatalyst.

4.1 Characterization Results

4.1.1 XRD

XRD patterns of Ti_3AlC_2, MX, MOF and MX/MOF were recorded to examine the crystal structure of materials (Fig 1). The characteristic peaks of Ti_3AlC_2 MAX precursor disappear in MX, showing successful exfoliation of MAX phase into MXenes (Fig S1). Absence of intense and sharp peaks for planes (004) and (104) at 19º and 39º marked for complete removal of Al through organic acid-assisted etching. Shifting of (002) peak from 9.49º to 7.08º in MX as compared to Ti_3AlC_2 MAX indicated increased interlayer spacing from 9.32 Å to 12.48 Å [28]. Moreover, the occurrence of new broad peaks showed the insertion of functional groups (-COOH), (=O), [14] and (-OH) after the removal of Al layers [51]. The characteristic peaks for MOF appear for planes (111), (200), (400) and (442) at 2θ=7.33º, 8.46 17.29 and 25.60, which are consistent with the literature [52]. This signifies that gel consists of crystalline components of 3D framework of UiO-66 structure. The broad and weak diffraction peaks reflected less crystalline structure of MOF particles. This is due to the higher concentration of reactants which led to faster nucleation rate and less crystalline structure i.e., amorphous structure. Moreover, the broadening of diffraction peaks indicated nanoparticles of MOF present in the gel [53]. This is further confirmed by the Debye-Scherrer equation; the average MOF's particle size was 28.83 nm. The MX/MOF peak shifted to a lower angle at 6.58º than pure MX and MOF at 7.08º and 7.33º. The peak shift showed increased d-spacing 13.44 Å in MX/MOF than 12.48 Å and 12.05 Å in MX and MOF. The heterostructure formed by growth of MOF particles on surface and between the layers of MX increased the interlayer spacing in MX/MOF. The occurrence of broad and less intensity peaks in composite is due to its amorphous structure.
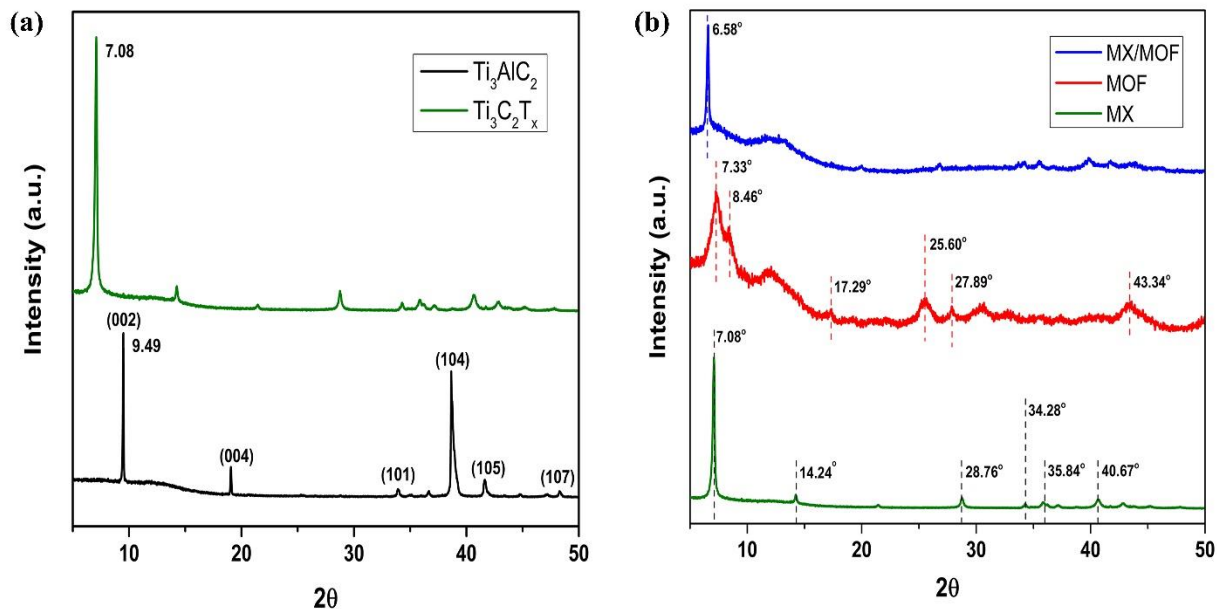
Figure 4.1: XRD of (a) Ti₃AlC₂ MAX phase and Ti₃C₂Tₓ (b) MX, MOF and MX/MOF composite.

The peak shift from 6.58^o in MX/MOF to 6.39^o in MX-1/MOF indicates increased d-spacing of 13.82 Å in MX-1/MOF than 13.44 Å in MX/MOF. It is due to growth of MOFs particles on MXenes surface. In this samples the ratio of MOFs is higher therefore more MOFs particles are grown on MXenes surface thus increasing its d-spacing. However, in sample MX-2/MOF the peak shifts towards higher angle of 6.59^o in MX-2/MOF than 6.58^o and 6.39^o in MX/MOF and MX-1/MOF. It has smaller d-spacing of 13.41 Å than other two composites. This is because MX-2/MOF has higher Ti₃C₂Tₓ MXenes concentration than MOFs particles grown on their surface, therefore less spacing between MXenes sheets is observed. Moreover, the characteristic peak for MX-1/MOF has lesser intensity than the characteristic peak of MX-2/MOF due to amount of MXenes in the samples.
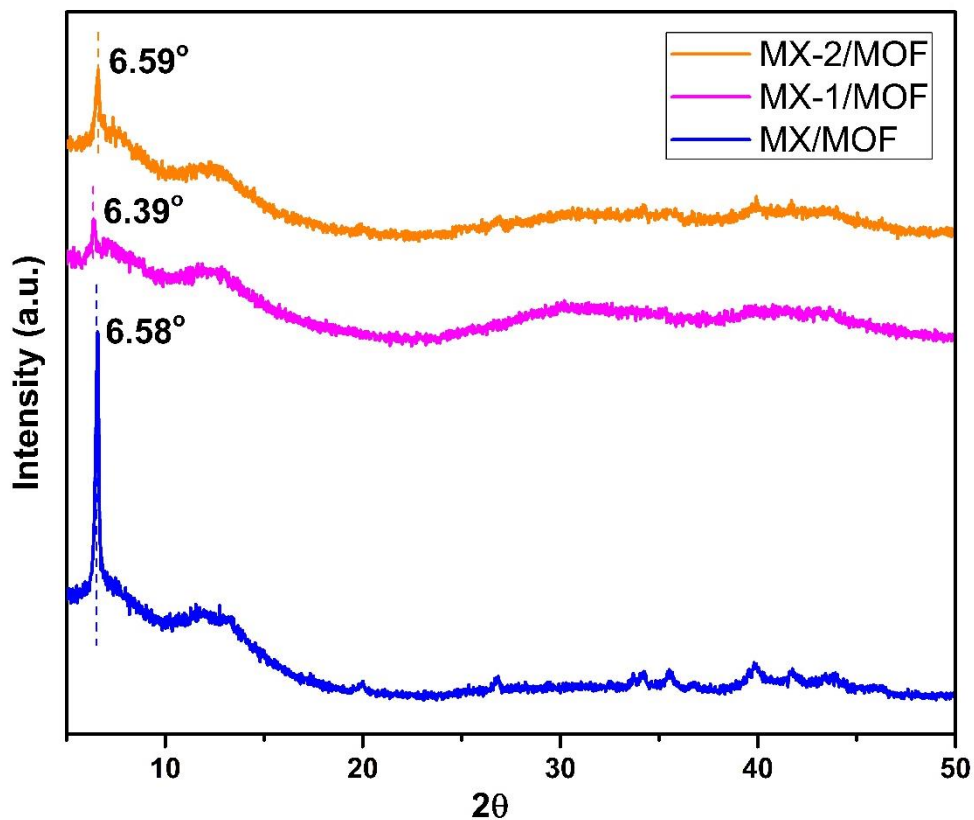
Figure 4.2: XRD of MX/MOF, MX-1/MOF and MX-2/MOF.

4.1.2 BET

BET adsorption-desorption isotherms were applied to calculate the specific surface area of MX, MOF and MX/MOF. The specific surface areas for MX, MOF and MX/MOF determined were 30.50 m^2/g, 393.70 m^2/g and 214.52 m^2/g respectively. MX has comparatively the lowest specific surface area due to its layered structure. The nano-sized particles of MOF had the highest surface area. The MX/MOF exhibited higher surface area tha pristine MX due to formation of composite with MOF. Moreover, the average pore radius of MX is 4.95 nm, MOF is 1.58 nm and MX/MOF is 1.28 nm.
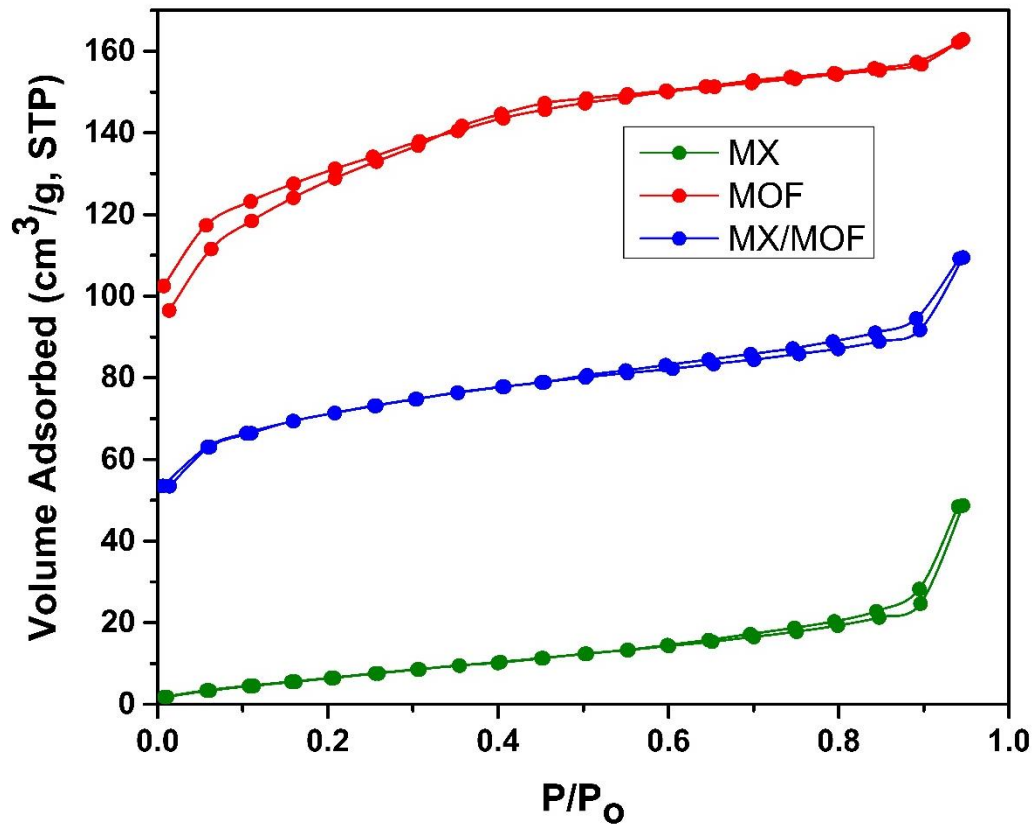
Figure 4.3: BET isotherms of MX, MOF and MX/MOF.

4.1.3 SEM

SEM was performed to analyze the morphology of materials. After etching of MAX phase the interlayer spacing between the MXenes's sheets is increased. The synthesized UIO-66 MOFs has gels network like structure. MOFs particles are grown on MXenes surface and forms an agglomerated structure.
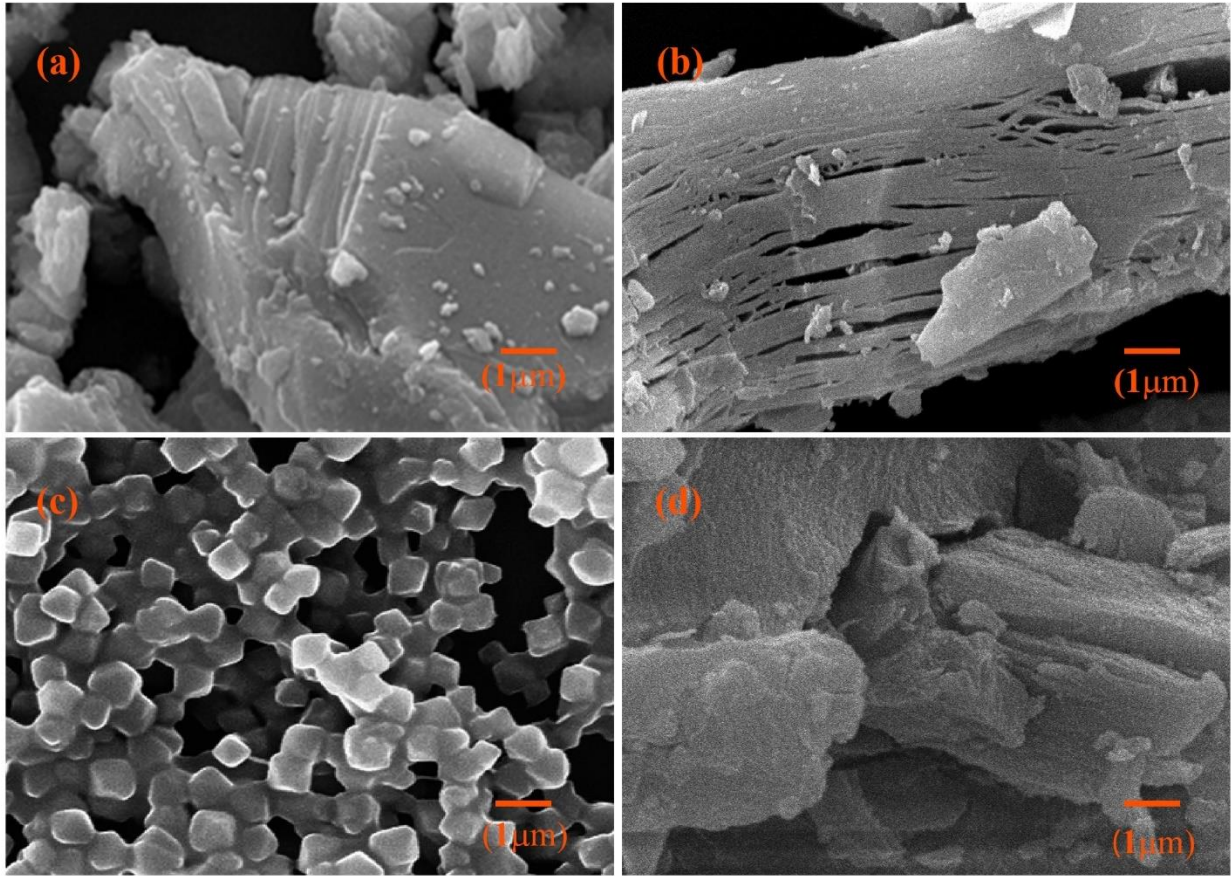
Figure 4.4: SEM of (a) MAX Phase (b) MX (c) MOF and (d) MX/MOF.

4.1.4 EDX

The elemental composition of MXenes, MOF and MX/MOF was determined by EDX analyzer, shown in table 1.

Table 4.1: EDX elemental composition of MXenes, MOF and MX/MOF

MXenes		MOF		MX/MOF	
Elements	Composition (%)	Elements	Composition (%)	Elements	Composition (%)
C	14.7	O	52.3	C	31.1
N	4.2	C	39.8	O	24.5
O	20.9	Zr	7.9	Ti	18.2
F	7.7			Zr	23.9
Ti	52.5			F	2.3

4.2 Electrochemical Testing Results

4.2.1 CV Curves

CV curves at 50 mV/s and 100 mV/s are shown in figure 4.5.

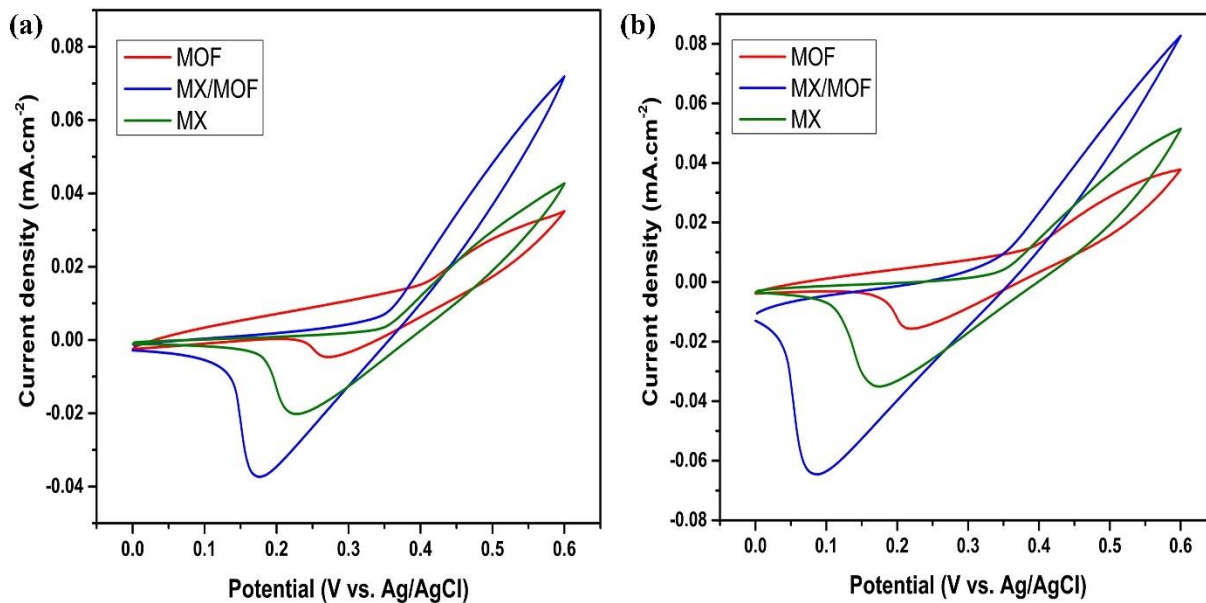**Figure 4.5:** CV curves of MX, MOF and MX/MOF at (a) 50 mV/s and (b) 100 mV/s scan rate.

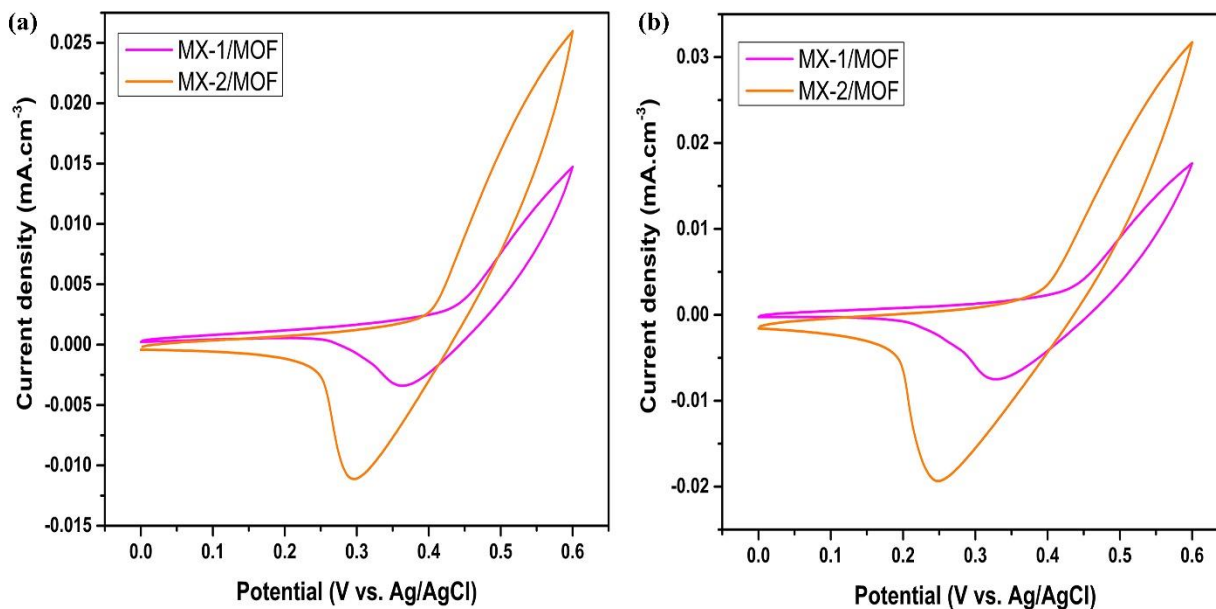CV curves of MX/MOF samples of varying mass ratios are at 50 mV/s and 100 mV/s are shown in figure 4.6.

Figure 4.6: CV curves of MX-1/MOF and MX-2/MOF at (a) 50 mV/s and (b) 100 mV/s scan rate.

4.2.2 Tafel Slope

Tafel slope is used to determine kinetics of process. A smaller Tafel slope means faster reaction kinetics, indicating that catalyst can achieve desired current at lower potential. The lowest overpotential amongst all samples was 86 mVdec^{-1} of MX-2/MOF. By increasing the concentration of MXenes in composite the reaction rates are increased, due to increased electrical conductivity of electrocatalyst.
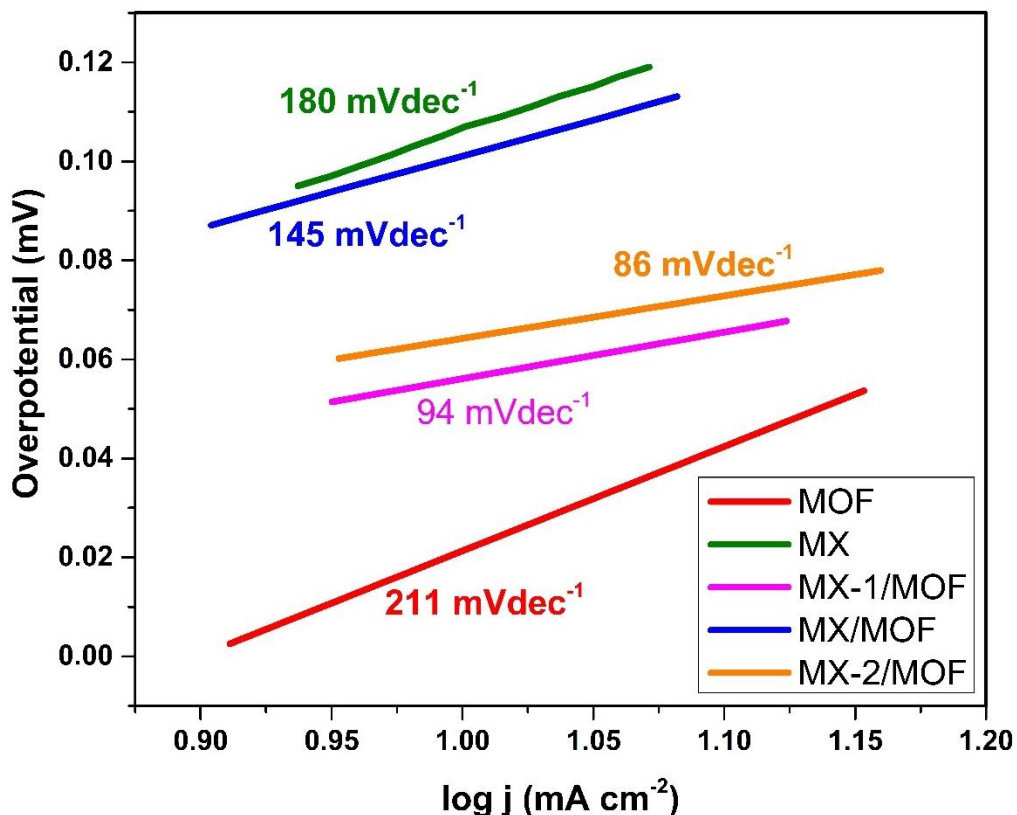
Figure 4.7: Tafel slopes of MOF, MX, MX/MOF, MX-1/MOF and MX-2/MOF.

4.2.3 HER

The electrocatalytic HER behavior of MX, MOF and MX/MOF were examined by three electrode system in 1 M KOH. The overpotential needed to achieve current density 10 mA cm^{-2} varied among prepared samples. The modifications in conventional synthesis of Ti$_3$C$_2$T$_x$ MXenes and UiO-66 MOFs done in this work are proven to be beneficial for electrocatalysis purpose and led a way forward for researchers. The introduction of -COOH functional groups on MXenes surface and the gel based UiO-66 MOFs' structure provided an increased number of active sites. Moreover, the MX/MOF composite has much less overpotential than pure MX and MOF which is 101 mV. The MX-2/MOF showed lowest overpotential amongst all, this is due to increase of

MXenes quantity in the composite. The high conductivity of mxenes resulted in lowering the overpotential. The introduction of -COOH functional groups on MXenes surface and the gel based UiO-66 MOFs' structure provided an increased number of active sites. The ability of MX/MOF electrocatalysts to achieve current density 10 mA cm^{-2} at this overpotential signifies that MX/MOF heterostructures enhanced HER active sites and increased electron transfer at MX/MOF interface. Table 4.2 show HER overpotential values for current density 10 mA cm^{-2}.

Figure 4.8: HER overpotential of MX, MOF, MX/MOF, MX-1/MOF and MX-2/MOF.

4.2.4   OER

The overpotential needed to achieve current density 10 mA cm^{-2} varied among prepared samples. The MX/MOF composite has much less overpotential than pure MX and MOF which is 80 mV. MX-2/MOF showed lowest overpotential which is 77 mV. The ability of MX/MOF electrocatalysts to achieve current density 10 mA cm^{-2} at this overpotential signifies that MX/MOF heterostructures enhanced OER active sites and increased electron transfer at MX/MOF interface. Table 4.2 shows OER overpotential values for 10 mA cm^{-2} current density.
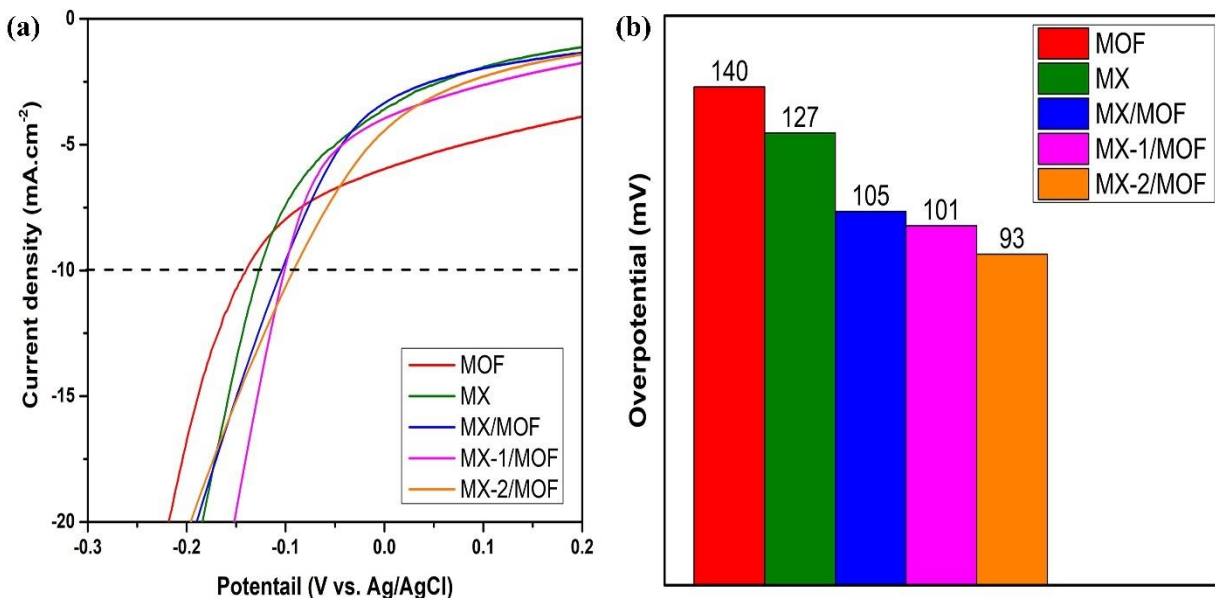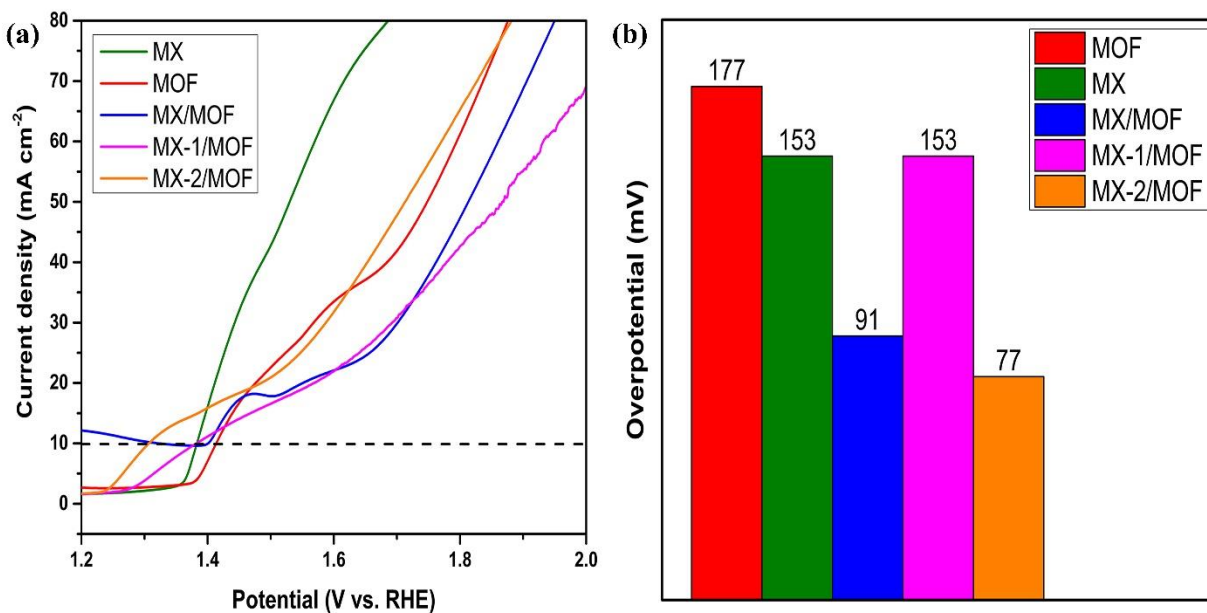
Figure 4.9: OER overpotential of MX, MOF, MX/MOF, MX-1/MOF and MX-2/MOF.

Table 4.2: HER and OER overpotentials.

	HER overpotential (mV)	OER overpotential (mV)
MX	140	177
MOF	127	153
MX/MOF	105	91
MX-1/MOF	101	153
MX-2/MOF	93	77

4.2.5   EIS

The electrochemical impedance spectroscopy results were analyzed using Gamry software. EIS was performed to determine the resistances, i.e., solution resistance and charge transfer resistance. Solution resistance is often a significant factor in the impedance of an electrochemical cell. A three electrode electrochemical cell accounts for the solution resistance between the counter and reference electrodes. It depends upon ionic concentration, type of ions, temperature, and the geometry of the area in which current is carried. Charge transfer resistance is formed by a single, kinetically controlled electrochemical reaction. During forward reaction, electrons enter the metal and metal ions diffuse into the electrolyte, causing charge to transfer with a certain speed. This

speed depends on reaction type, temperature, concentration of the reaction products and the potential. Warburg impedance is created due to diffusion and depends on the frequency of the potential perturbation. At high frequencies, it is small because diffusing reactants don't have to move very far. At low frequencies, the reactants must diffuse farther, increasing the Warburg-impedance. The figure 4.10 shows Nyquist plot of pure MX and MOF and the composite MX/MOF.
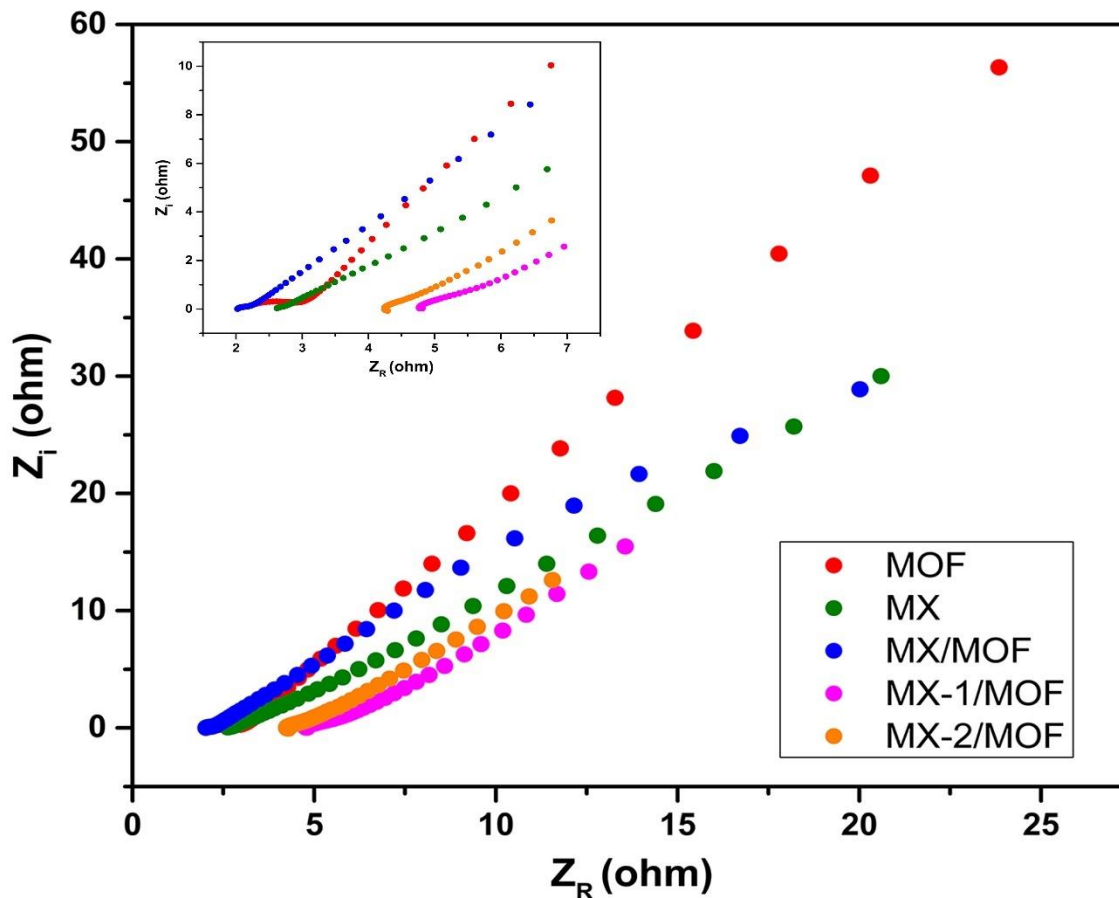
Figure 4.10: EIS plot of MOF, MX, MX/MOF, MX-1/MOF and MX-2/MOF.

Table 4.3 show the value of resistances. The charge transfer resistance for MX-2/MOF is lowest, which indicated higher HER kinetics of the composite.

Table 4.3: EIS parameters of MOF, MX and MX/MOF.

Parameters	MOF	MX	MX/MOF	MX-1/MOF	MX-2/MOF
Solution resistance (R_s, Ω)	2.520	2.554	2.011	4.529	4.03
Capacitance (C, F)	2.5×10^{-3}	8.73×10^{-3}	5.93×10^{-3}	1.78×10^{-3}	1.69×10^{-3}

Charge transfer resistance (R_{CT}, Ω)	218.5	60.57	48.81	5.948	3.86
Warburg Resistance ($\Omega s^{-1/2}$)	19.54×10^{-3}	19.55×10^{-3}	29.16×10^{-3}	5.88×10^{-3}	7.074×10^{-3}

4.2.6 Electrocatalyst Stability

The MX-2/MOF had the lowest overpotential for HER. Therefore, the electrocatalyst was subjected to analyze its stability. Stability of electrocatalyst was determined through chronopotentiometry at 10 mA. The catalyst showed a stable behaviour due its structure. The response was constant without any significant change loss in activity.
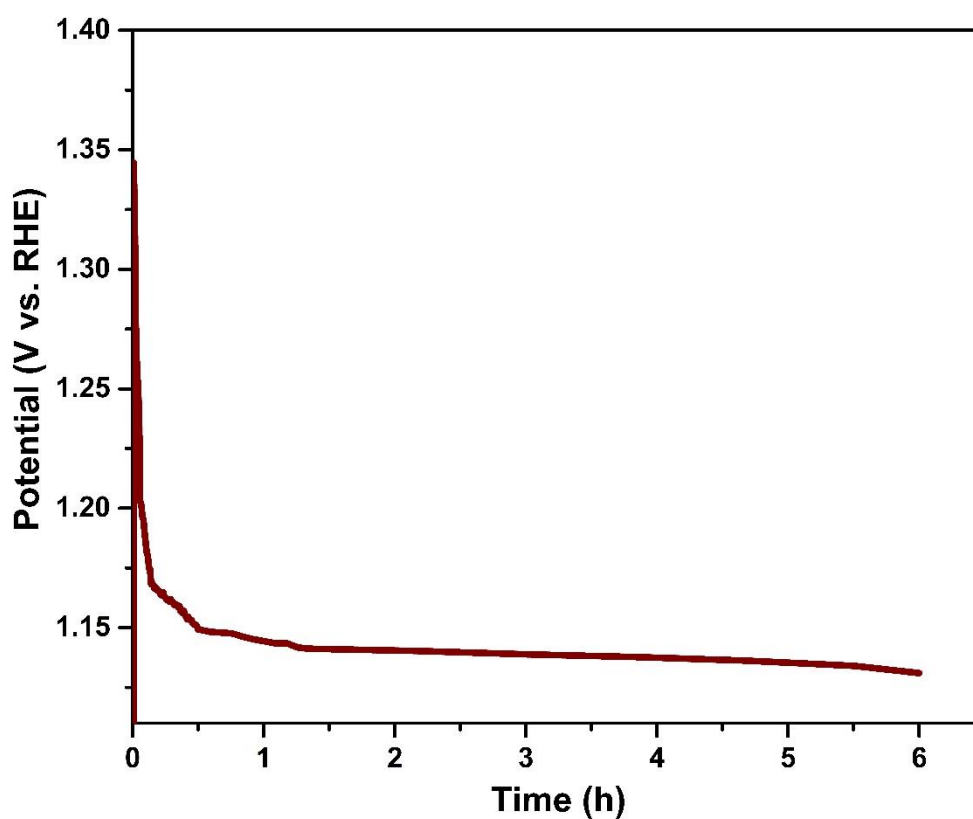

Figure 4.11: Chronopotentiometry curve for MX-2/MOF at 10 mA.

Conclusion

The study was aimed to synthesize a $Ti_3C_2T_x$ MXenes based electrocatalyst for optimum H_2 production through water electrolysis. $Ti_3C_2T_x$ MXenes/UiO-66 MOFs composite was selected as material for electrocatalyst for HER. In this work the $Ti_3C_2T_x$ MXenes were modifies as $Ti_3C_2T_x$-(COOH) through etching with NH_4HF_2 and citric acid. Occurrence of -COOH groups on MXenes surface increased their conductivity and enhanced their electrochemical activity. Three different composites of varying $Ti_3C_2T_x$ MXenes:UiO-66 MOFs mass ratios of 1:1, 1:2 and 2:1 were synthesized. The electrochemical testing results showed that the MX-2/MOF had lowest HER and OER potentials of 93 and 77 mV respectively. Moreover, the electrocatalyst had lowest Tafel slope of 86 $mVdec^{-1}$. The catalyst was highly stable and retained its activity even after 6h. Thus, $Ti_3C_2T_x$ MXenes/UiO-66 MOFs composites can serve for electrocatalytic H_2 production.

Recommendations

1. The high conductivity of MXenes make them potentially applicable in energy storage and energy conversion devices. MXenes other than $Ti_3C_2T_x$, can be as electrocatalyst for H_2 production through making their composites with UiO-66 MOFs or other Zr based MOFs.

2. The modification of MXenes done in this work can open ways for modification of Mxenes through various etchants can increase their HER activity. Therefore, in future MXenes can be modified through etching with other carboxylated acids and can be tested for HER activity.

3. The synthesis method used in this work was in-situ approach. However, the same composites can be synthesized by mixing approach. The effect of synthesis method can be analyzed and compared with this work.

References

[1]   A. Sinopoli, Z. Othman, K. Rasool, K. A. J. C. O. i. S. S. Mahmoud, and M. Science, "Electrocatalytic/photocatalytic properties and aqueous media applications of 2D transition metal carbides (MXenes)," vol. 23, no. 5, p. 100760, 2019.

[2]   X. Bai and J. J. C. J. o. C. Guan, "MXenes for electrocatalysis applications: Modification and hybridization," vol. 43, no. 8, pp. 2057-2090, 2022.

[3]   L. Baharudin and M. J. R. i. C. E. James Watson, "Hydrogen applications and research activities in its production routes through catalytic hydrocarbon conversion," vol. 34, no. 1, pp. 43-72, 2017.

[4]   H. G. M.-b. Merchant and C. J. A. a. h. a. p. c. h.-g.-m.-b.-m.-c.-d.-c.-. Type, "Distributed & Centralized Generation, Application & Technology-Trends & Global Forecasts (2011-2016)," vol. 561523, 2011.

[5]   A. Whiteman, "Global trends and outlook for forest resources," in *Challenges and Opportunities for the World's Forests in the 21st Century*: Springer, 2013, pp. 163-211.

[6]   H. Nazir *et al.*, "Is the H2 economy realizable in the foreseeable future? Part III: H2 usage technologies, applications, and challenges and opportunities," vol. 45, no. 53, pp. 28217-28239, 2020.

[7]   S. Bajracharya, "Microbial Electrosynthesis of Biochemicals: Innovations on Biocatalysts, Electrodes and Ion-Exchange for CO 2 Supply, Chemicals Production and Separation," Wageningen University and Research, 2016.

[8]   Y. Wei, R. A. Soomro, X. Xie, and B. J. J. o. E. C. Xu, "Design of efficient electrocatalysts for hydrogen evolution reaction based on 2D MXenes," vol. 55, pp. 244-255, 2021.

[9]   E. Maleeva, K. Pedan, and V. J. R. j. o. e. Kudryavtsev, "The mechanism of cathodic hydrogen evolution and its entry into iron and the determination of the cathode surface coverage with hydrogen adatoms in alkaline solutions," vol. 32, no. 7, pp. 770-777, 1996.

[10]   A. J. J. N. Bard, "Between electrode and solution," vol. 368, no. 6472, pp. 597-598, 1994.

[11]   X. Zhong *et al.*, "3D heterostructured pure and N-Doped Ni3S2/VS2 nanosheets for high efficient overall water splitting," vol. 269, pp. 55-61, 2018.

[12]   M. Zeng and Y. J. J. o. M. C. A. Li, "Recent advances in heterogeneous electrocatalysts for the hydrogen evolution reaction," vol. 3, no. 29, pp. 14942-14962, 2015.

[13]   X. Zhong *et al.*, "Efficient coupling of a hierarchical V 2 O 5@ Ni 3 S 2 hybrid nanoarray for pseudocapacitors and hydrogen production," vol. 5, no. 34, pp. 17954-17962, 2017.

[14]   W.-F. Chen, J. T. Muckerman, and E. J. C. c. Fujita, "Recent developments in transition metal carbides and nitrides as hydrogen evolution electrocatalysts," vol. 49, no. 79, pp. 8896-8909, 2013.

[15]   Y. Qu *et al.*, "Facile synthesis of vanadium-doped Ni3S2 nanowire arrays as active electrocatalyst for hydrogen evolution reaction," vol. 9, no. 7, pp. 5959-5967, 2017.

[16]   J. Greeley, T. F. Jaramillo, J. Bonde, I. Chorkendorff, and J. K. J. N. m. Nørskov, "Computational high-throughput screening of electrocatalytic materials for hydrogen evolution," vol. 5, no. 11, pp. 909-913, 2006.

[17]   J. K. Nørskov *et al.*, "Trends in the exchange current for hydrogen evolution," vol. 152, no. 3, p. J23, 2005.

[18]   X. Bai, C. Ling, L. Shi, Y. Ouyang, Q. Li, and J. J. S. B. Wang, "Insight into the catalytic activity of MXenes for hydrogen evolution reaction," vol. 63, no. 21, pp. 1397-1403, 2018.

[19]   Z. Seh, J. Kibsgaard, C. Dickens, I. Chorkendorff, J. Nørskov, and T. Jaramillo, "Combining theory and experiment in electrocatalysis: insights into materials design. Science 355: eaad4998," ed, 2017.

[20]   Y. Shi and B. J. C. S. R. Zhang, "Recent advances in transition metal phosphide nanomaterials: synthesis and applications in hydrogen evolution reaction," vol. 45, no. 6, pp. 1529-1541, 2016.

[21]   H. Lin *et al.*, "Heteronanowires of MoC–Mo 2 C as efficient electrocatalysts for hydrogen evolution reaction," vol. 7, no. 5, pp. 3399-3405, 2016.

[22]   Z. Chen *et al.*, "Tailoring the d-band centers enables Co4N nanosheets to be highly active for hydrogen evolution catalysis," vol. 130, no. 18, pp. 5170-5174, 2018.

[23]   Q. Wang *et al.*, "Free-standing phosphorous-doped molybdenum nitride in 3D carbon nanosheet towards hydrogen evolution at all pH values," vol. 50, pp. 44-51, 2020.

[24]   Y. Gogotsi and B. J. A. n. Anasori, "The rise of MXenes," vol. 13, ed: ACS Publications, 2019, pp. 8491-8494.

[25]   K. A. Papadopoulou, A. Chroneos, D. Parfitt, and S.-R. G. J. J. o. A. P. Christopoulos, "A perspective on MXenes: Their synthesis, properties, and recent applications," vol. 128, no. 17, p. 170902, 2020.

[26]   H. H. Do *et al.*, "Metal-organic-framework based catalyst for hydrogen production: Progress and perspectives," 2022.

[27]   Y. Bai, Y. Dou, L.-H. Xie, W. Rutledge, J.-R. Li, and H.-C. J. C. S. R. Zhou, "Zr-based metal–organic frameworks: design, synthesis, structure, and applications," vol. 45, no. 8, pp. 2327-2367, 2016.

[28]   L. Zhao *et al.*, "Interdiffusion reaction-assisted hybridization of two-dimensional metal–organic frameworks and Ti3C2T x nanosheets for electrocatalytic oxygen evolution," vol. 11, no. 6, pp. 5800-5807, 2017.

[29]   J. Qin *et al.*, "0D/2D MXene quantum dot/Ni-MOF ultrathin nanosheets for enhanced N2 photoreduction," vol. 8, no. 48, pp. 17791-17799, 2020.

[30]   C. F. Du *et al.*, "Self-assemble and in situ formation of Ni1− xFexPS3 nanomosaic-decorated MXene hybrids for overall water splitting," vol. 8, no. 26, p. 1801127, 2018.

[31]   Y. Wen, Z. Wei, C. Ma, X. Xing, Z. Li, and D. J. N. Luo, "MXene boosted CoNi-ZIF-67 as highly efficient electrocatalysts for oxygen evolution," vol. 9, no. 5, p. 775, 2019.

[32]   W. Zhao *et al.*, "Interlayer hydrogen-bonded metal porphyrin frameworks/MXene hybrid film with high capacitance for flexible all-solid-state supercapacitors," vol. 15, no. 18, p. 1901351, 2019.

[33]   S. Zhao, R. Nivetha, Y. Qiu, and X. J. C. C. L. Guo, "Two-dimensional hybrid nanomaterials derived from MXenes (Ti3C2Tx) as advanced energy storage and conversion applications," vol. 31, no. 4, pp. 947-952, 2020.

[34]   Y. Yuan *et al.*, "Achieving highly efficient catalysts for hydrogen evolution reaction by electronic state modification of platinum on versatile Ti3C2T x (MXene)," vol. 7, no. 4, pp. 4266-4273, 2019.

[35]   X. Zhang *et al.*, "Platinum Nanoparticle-Deposited Ti3C2T x MXene for Hydrogen Evolution Reaction," vol. 59, no. 5, pp. 1822-1828, 2020.

[36]   C. Cui, R. Cheng, C. Zhang, and X. J. C. C. L. Wang, "Pt immobilized spontaneously on porous MXene/MAX hybrid monolith for hydrogen evolution reaction," vol. 31, no. 4, pp. 988-991, 2020.

[37]   C. Cui *et al.*, "Ultrastable MXene@ Pt/SWCNTs' nanocatalysts for hydrogen evolution reaction," vol. 30, no. 47, p. 2000693, 2020.

[38] H. Yin *et al.*, "Ultrathin platinum nanowires grown on single-layered nickel hydroxide with high hydrogen evolution activity," vol. 6, no. 1, pp. 1-8, 2015.

[39] Y. Jiao, Y. Zheng, M. Jaroniec, and S. Z. J. C. S. R. Qiao, "Design of electrocatalysts for oxygen-and hydrogen-involving energy conversion reactions," vol. 44, no. 8, pp. 2060-2086, 2015.

[40] Z. Peng and H. J. N. t. Yang, "Designer platinum nanoparticles: Control of shape, composition in alloy, nanostructure and electrocatalytic property," vol. 4, no. 2, pp. 143-164, 2009.

[41] J. Peng, X. Chen, W.-J. Ong, X. Zhao, and N. J. C. Li, "Surface and heterointerface engineering of 2D MXenes and their nanocomposites: insights into electro-and photocatalysis," vol. 5, no. 1, pp. 18-50, 2019.

[42] Z. Li *et al.*, "In situ formed Pt3Ti nanoparticles on a two-dimensional transition metal carbide (MXene) used as efficient catalysts for hydrogen evolution reactions," vol. 19, no. 8, pp. 5102-5108, 2019.

[43] X. Wu, Z. Wang, M. Yu, L. Xiu, and J. J. A. M. Qiu, "Stabilizing the MXenes by carbon nanoplating for developing hierarchical nanohybrids with efficient lithium storage and hydrogen evolution capability," vol. 29, no. 24, p. 1607017, 2017.

[44] N. H. Attanayake *et al.*, "Vertically aligned MoS 2 on Ti 3 C 2 (MXene) as an improved HER catalyst," vol. 6, no. 35, pp. 16882-16889, 2018.

[45] L. Hu, Y. Sun, S.-J. Gong, H. Zong, K. Yu, and Z. J. N. J. o. C. Zhu, "Experimental and theoretical investigation on MoS 2/MXene heterostructure as an efficient electrocatalyst for hydrogen evolution in both acidic and alkaline media," vol. 44, no. 19, pp. 7902-7911, 2020.

[46] C. Ling, L. Shi, Y. Ouyang, Q. Chen, and J. J. A. S. Wang, "Transition metal-promoted V2CO2 (MXenes): a new and highly active catalyst for hydrogen evolution reaction," vol. 3, no. 11, p. 1600180, 2016.

[47] J. Zhang *et al.*, "Single platinum atoms immobilized on an MXene as an efficient catalyst for the hydrogen evolution reaction," vol. 1, no. 12, pp. 985-992, 2018.

[48] Y. Jiang *et al.*, "Coupling PtNi ultrathin nanowires with MXenes for boosting electrocatalytic hydrogen evolution in both acidic and alkaline solutions," vol. 15, no. 12, p. 1805474, 2019.

[49] H. Zou, B. He, P. Kuang, J. Yu, K. J. A. a. m. Fan, and interfaces, "Metal–organic framework-derived nickel–cobalt sulfide on ultrathin mxene nanosheets for electrocatalytic oxygen evolution," vol. 10, no. 26, pp. 22311-22319, 2018.

[50] L. He *et al.*, "Cobalt oxide doped with titanium dioxide and embedded with carbon nanotubes and graphene-like nanosheets for efficient trifunctional electrocatalyst of hydrogen evolution, oxygen reduction, and oxygen evolution reaction," vol. 414, pp. 333-344, 2019.

[51] M. Li *et al.*, "Element replacement approach by reaction with Lewis acidic molten salts to synthesize nanolaminated MAX phases and MXenes," vol. 141, no. 11, pp. 4730-4737, 2019.

[52] T. Sai *et al.*, "Deposition growth of Zr-based MOFs on cerium phenylphosphonate lamella towards enhanced thermal stability and fire safety of polycarbonate," *Composites Part B: Engineering,* vol. 197, p. 108064, 2020/09/15/ 2020.

[53] X. Feng *et al.*, "Trace-doped metal–organic gels with remarkably enhanced luminescence," vol. 7, no. 59, pp. 37194-37199, 2017.